Neuron

Article

Amygdala-Midbrain Connections Modulate Appetitive and Aversive Learning

Graphical Abstract

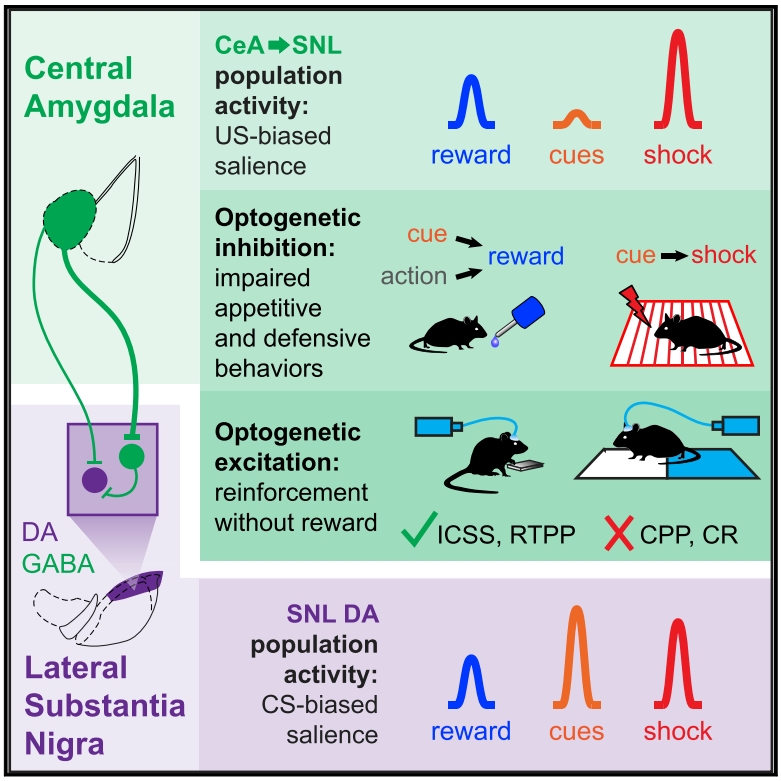

Highlights

- CeA→SNL populations encode a salience signal biased to unconditioned stimuli
- CeA→SNL activity is necessary for conditioned reward-seeking and defensive behaviors
- CeA cells form monosynaptic connections with nigral GABA and dopamine neurons
- SNL dopamine populations encode a salience signal biased to conditioned stimuli

Authors

Elizabeth E. Steinberg, Felicity Gore, Boris D. Heifets, ..., Liqun Luo, Karl Deisseroth, Robert C. Malenka

Correspondence

malenka@stanford.edu

In Brief

Steinberg et al. investigate how connections between the central amygdala and the lateral substantia nigra contribute to emotional behaviors. They find that amygdalonigral neurons are activated by salient stimuli and participate in appetitive and aversive learning via connections with nigral GABA and dopamine neurons.

Steinberg et al., 2020, Neuron *106*, 1026–1043
June 17, 2020
https://doi.org/10.1016/j.neuron.2020.03.016

CellPress

CellPress

Neuron

Article

Amygdala-Midbrain Connections Modulate Appetitive and Aversive Learning

Elizabeth E. Steinberg,[1] Felicity Gore,[1,2] Boris D. Heifets,[1,3] Madison D. Taylor,[1] Zane C. Norville,[1] Kevin T. Beier,[1,4,6] Csaba Földy,[1,5] Talia N. Lerner,[2,7] Liqun Luo,[4] Karl Deisseroth,[2] and Robert C. Malenka[1,8,*]

[1]Nancy Pritzker Laboratory, Department of Psychiatry & Behavioral Sciences, Stanford University, Stanford, CA 94305, USA
[2]Departments of Bioengineering and Psychiatry and Howard Hughes Medical Institute, Stanford University, Stanford, CA 94305, USA
[3]Department of Anesthesiology, Stanford University, Stanford, CA 94305, USA
[4]Department of Biology and Howard Hughes Medical Institute, Stanford University, Stanford, CA 94305, USA
[5]Brain Research Institute, University of Zurich, Zurich, Switzerland
[6]Present address: Department of Physiology and Biophysics, University of California, Irvine, Irvine, CA 92617, USA
[7]Present address: Department of Physiology, Northwestern University, Chicago, IL 60611, USA
[8]Lead Contact
*Correspondence: malenka@stanford.edu
https://doi.org/10.1016/j.neuron.2020.03.016

SUMMARY

The central amygdala (CeA) orchestrates adaptive responses to emotional events. While CeA substrates for defensive behaviors have been studied extensively, CeA circuits for appetitive behaviors and their relationship to threat-responsive circuits remain poorly defined. Here, we demonstrate that the CeA sends robust inhibitory projections to the lateral substantia nigra (SNL) that contribute to appetitive and aversive learning in mice. CeA→SNL neural responses to appetitive and aversive stimuli were modulated by expectation and magnitude consistent with a population-level salience signal, which was required for Pavlovian conditioned reward-seeking and defensive behaviors. CeA→SNL terminal activation elicited reinforcement when linked to voluntary actions but failed to support Pavlovian associations that rely on incentive value signals. Consistent with a disinhibitory mechanism, CeA inputs preferentially target SNL GABA neurons, and CeA→SNL and SNL dopamine neurons respond similarly to salient stimuli. Collectively, our results suggest that amygdala-nigra interactions represent a previously unappreciated mechanism for influencing emotional behaviors.

INTRODUCTION

The amygdala is an evolutionarily conserved hub for emotional processing, with homologous structure and function observed across vertebrate species (Janak and Tye, 2015). Its role in conferring motivational significance to neutral stimuli though associative learning has been well established, especially in the context of aversive events (Phelps and LeDoux, 2005). The amygdala contains multiple subregions, including the central amygdala (CeA), a GABAergic nucleus that is essential for the autonomic and behavioral changes evoked by threatening stimuli (Davis, 1992). Recently, a detailed picture of CeA circuits that mediate defensive behaviors has emerged, with functional roles ascribed to genetically defined cell types and local microcircuits, as well as long-range afferent and efferent connections (Fadok et al., 2018; Li, 2019).

In addition to regulating responses to threat, the amygdala contributes to other cognitive processes, including reward learning (Weiskrantz, 1956; Holland and Gallagher, 1999), which encompasses two classes of associative relationships: instrumental learning about the consequences of voluntary actions, and Pavlovian learning about predictive cues. These parallel processes interact in complex ways and are thought to depend on overlapping but distinct neural substrates (O'Doherty et al., 2017). The CeA has been implicated in both instrumental and Pavlovian reward learning (Gallagher et al., 1990; Holland and Gallagher, 1993; Corbit and Balleine, 2005; Lingawi and Balleine, 2012; Robinson et al., 2014), but the efferent pathways involved, and their relationship to circuits that participate in defensive behaviors, remain unclear.

In rats and non-human primates, the CeA sends a projection to the lateral substantia nigra (SNL), which constitutes the major direct communication channel from the amygdala to midbrain dopamine (DA) regions (Vankova et al., 1992; Fudge and Haber, 2000). Midbrain DA neurons perform essential roles in reward-motivated behavior (Berridge and Robinson, 1998; Steinberg and Janak, 2013; Schultz, 2016), with most work focusing on ventral tegmental area (VTA) DA neurons. Less is known about the contribution of SNL DA neurons, which appear to have unusual response properties related to salience, novelty, and stimulus intensity (Matsumoto and Hikosaka, 2009; Lerner et al., 2015; Menegas et al., 2017, 2018). Thus, we hypothesized that CeA signals could convey information about salient stimuli to a unique DA subpopulation to modulate behavioral responses to reward and threat.

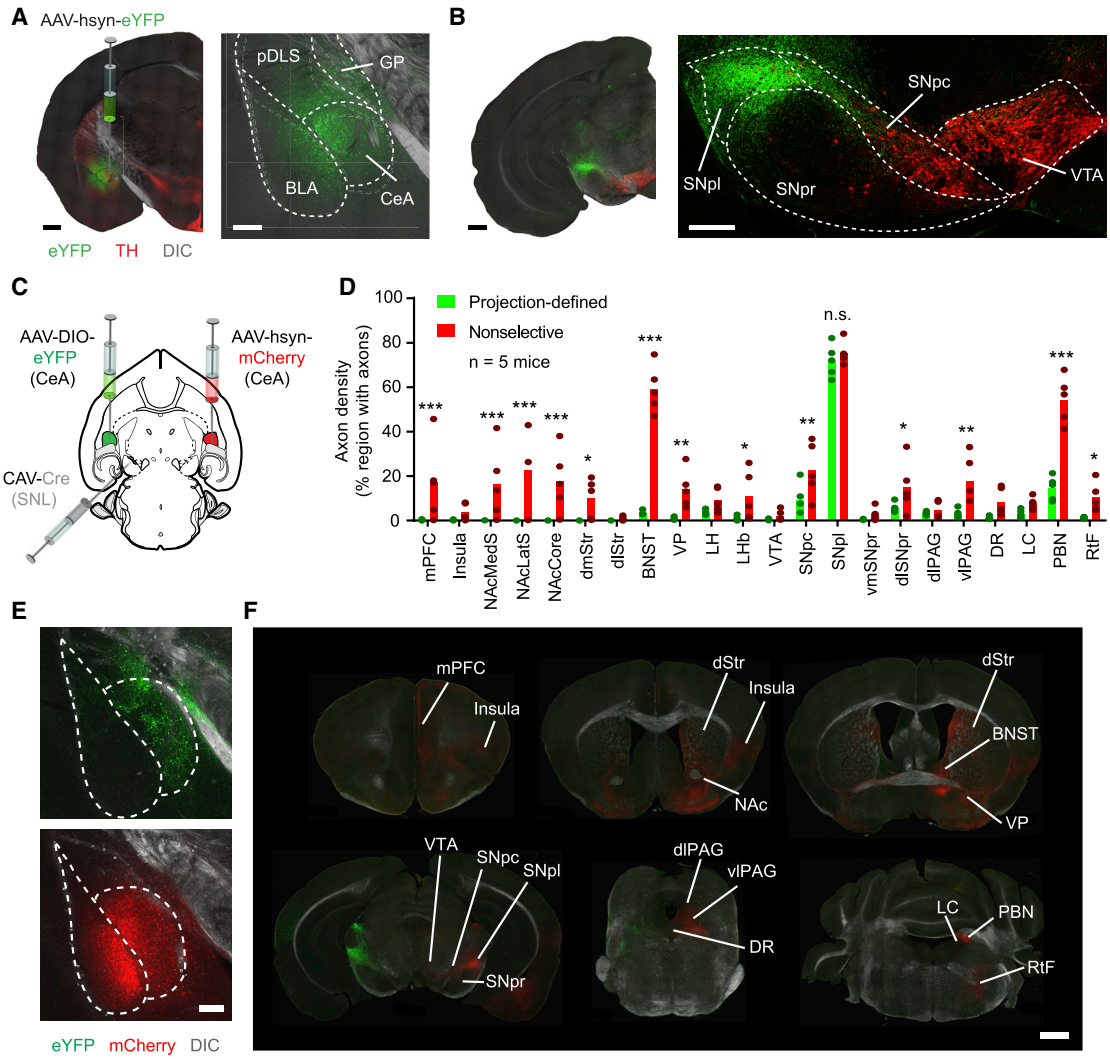

Figure 1. CeA-Midbrain Projections Have a Lateral Bias and Do Not Collateralize Extensively

(A) CeA injection site at low and high magnification (scale bar, 500/250 μm). TH, tyrosine hydroxylase; DIC, differential interference contrast.

(B) CeA terminals in midbrain DA regions at low and high magnification (scale bar, 500/250 μm).

(C) Strategy for axon collateralization analysis.

(D) Quantification of axon density (percentage of region containing pixels above threshold; n = 5 mice).

(E) CeA injection sites (scale bar, 250 μm).

(F) CeA→SNL axons (green) and non-selective amygdala axons (red) (scale bar, 1 mm).

CeA, central amygdala; BLA, basolateral amygdala; pDLS, posterior dorsolateral striatum; GP, globus pallidus; mPFC, medial prefrontal cortex; insula, insular cortex; NAcMedS, NAcLatS, NAcCore, nucleus accumbens medial shell, lateral shell, core; dmStr, dlStr, dorsomedial and dorsolateral striatum; BNST, bed nucleus of stria terminalis; VP, ventral pallidum; LH, lateral hypothalamus; LHb, lateral habenula; VTA, ventral tegmental area; SNpc, substantia nigra pars compacta; SNpl, substantia nigra pars lateralis; vmSNpr, dlSNpr, ventromedial and dorsolateral substantia nigra pars reticulata; dlPAG, vlPAG, dorsolateral and ventrolateral periaqueductal gray; DR, dorsal raphae; LC, locus coeruleus; PBN, parabrachial nucleus; RtF, reticular formation.

*p < 0.05; **p < 0.01; ***p < 0.001.

See also Figure S1 and Table S1 for statistical details.

RESULTS

A Population of CeA Neurons that Preferentially Target SNL

CeA→SNL projections have not been carefully examined in the mouse using contemporary methodologies. Thus, we employed viral tracing to visualize inputs from the amygdala to midbrain DA regions in wild-type mice. We injected an adeno-associated virus (AAV) expressing eYFP into the CeA (Figures 1A and 1B) and found that CeA-midbrain projections were laterally biased, with dense terminals in the substantia nigra pars lateralis (SNpl) and lateral portions of the substantia nigra pars compacta (SNpc), the combination of which we define as SNL. To determine which regions of the amygdala give rise to SNL projections,

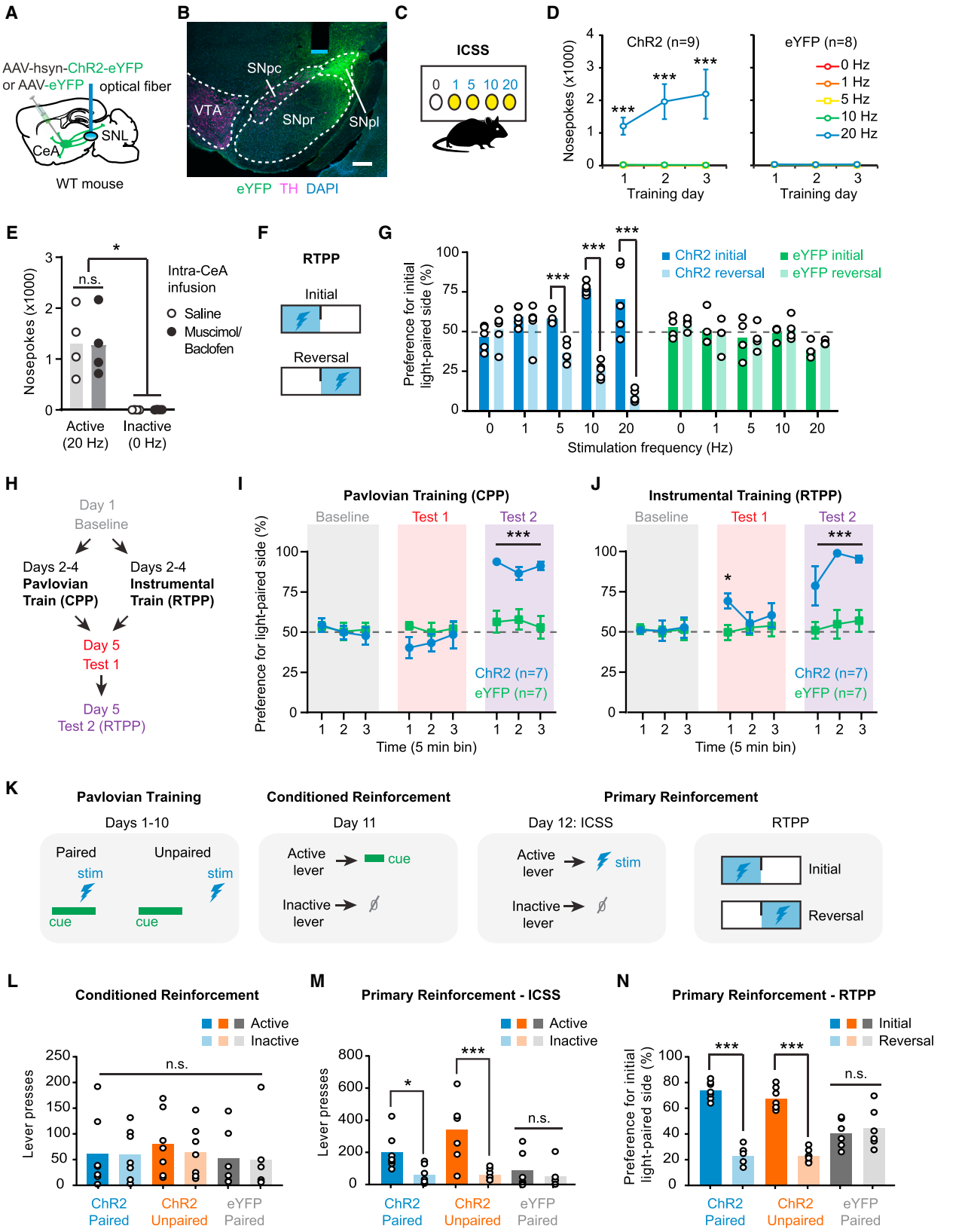

(legend on next page)

we injected a retrograde canine adenovirus expressing Cre recombinase (CAV-Cre) into SNL of Ai14 Cre-reporter mice (Madisen et al., 2010) (Figures S1A–S1C). Labeled cells were found throughout the anterior-posterior extent of the CeA, including medial and lateral subdivisions (Figure S1D), with the highest density in posterior lateral CeA. Labeled cells were also found in the overlying striatum including the adjacent amygdalostriatal transition area and posterior dorsolateral striatum (DLS). Consistent with reports in other species, few labeled cells were seen in basolateral amygdala (BLA). Thus, in mice, the CeA sends a robust projection to midbrain DA regions, which is structured to differentially influence neural activity across lateral-to-medial gradients.

Do CeA→SNL neurons project primarily to SNL, or do they have robust axon collaterals that target multiple regions? We used an intersectional viral strategy to selectively label CeA→SNL neurons ("projection-defined condition"), injecting CAV-Cre into the SNL and a Cre-dependent AAV-eYFP into the CeA (Schwarz et al., 2015), and examined axon density in 22 brain regions (Figure 1C). For comparison, in the other hemisphere, we injected AAV-mCherry into the CeA ("nonselective condition"). SNpl axon density was similarly high in both projection-defined and nonselective conditions (Figures 1D–1F; $p = 0.447$; for full statistical information, see Table S1), indicating that the majority of the CeA→SNL pathway was sampled in the projection-defined condition. Importantly, the density of CeA axons within SNpl for the projection-defined condition was at least five times greater than any other region examined (SNpl versus all other regions $p < 0.05$). Furthermore, there were differences between the density of projection-defined and nonselective labeling in all regions receiving at least 10% coverage in the nonselective condition, indicating that CeA neurons that comprise these pathways only modestly overlap with CeA→SNL neurons ($p < 0.05$). Thus, CeA→SNL neurons do not collateralize extensively.

CeA→SNL Projections Reinforce a Subset of Associations Supported by Natural Rewards

Because midbrain DA neurons are strongly implicated in reward learning (Berridge and Robinson, 1998; Steinberg and Janak, 2013; Schultz, 2016), we hypothesized that CeA→SNL projections would modulate appetitive behaviors. As an initial test of this hypothesis, we asked whether CeA→SNL pathway activation was sufficient to reinforce instrumental associations, given that direct activation of VTA or SNc DA neurons robustly drives positive reinforcement (Saunders et al., 2018). We injected AAV-ChR2 or AAV-eYFP into the CeA in wild-type mice and implanted an optical fiber above the SNL (Figures 2A, 2B, and S2A). Mice were allowed to nosepoke for bilateral optical stimulation at different frequencies (Figure 2C). ChR2 mice quickly developed robust intracranial self-stimulation (ICSS) behavior for 20-Hz stimulation (Figure 2D; $p < 0.001$), whereas control mice did not (Figure 2D; $p > 0.059$). To determine if antidromic activation of CeA cell bodies contributed to ICSS, we infused GABA-A/GABA-B agonists (muscimol/baclofen) into the CeA to inactivate this structure (Figures 2E and S2B). ICSS response rates were similar with the CeA intact or inactivated ($p > 0.884$), indicating that activation of CeA→SNL terminals generates reinforcement that is driven by local effects within SNL.

To examine whether CeA→SNL projections support other forms of positive reinforcement, we assayed instrumental place preference (i.e., real-time place preference [RTPP]; Figure 2F). ChR2 mice exhibited a strong preference for the compartment paired with 5-, 10-, or 20-Hz stimulation that reversed when contingencies changed (Figure 2G; $p < 0.001$), while light delivery did not influence control mice ($p > 0.146$). CeA→SNL RTPP was similarly robust in mice of both sexes (Figure S2C; no effect of sex, $p = 0.299$). Open field tests revealed that bilateral 10- and 20-Hz stimulation decreased locomotion (Figure S2D). However, unilateral stimulation did not affect locomotion (Figure S2E) and still robustly supported ICSS and RTPP (Figures S2F and S2G), indicating that changes in locomotion cannot explain the positive reinforcement we observed.

Natural rewards support Pavlovian associations as well as reinforcing instrumental behavior. During Pavlovian reward learning, stimuli acquire incentive value and promote approach in the absence of the primary reward (Everitt et al., 1991), sustaining reward pursuit when reward is not immediately available. To determine if CeA→SNL pathway activation supports Pavlovian learning, we performed a conditioned place

Figure 2. CeA→SNL Neurons Reinforce Instrumental but Not Pavlovian Associations

(A) Strategy for activating CeA→SNL projections.
(B) Representative histology. Blue line indicates fiber tip (scale bar, 200 μm).
(C) Schematic of the five-choice ICSS task.
(D) ChR2, but not eYFP, mice respond for optogenetic stimulation.
(E) CeA inactivation does not impair ICSS for CeA→SNL terminal stimulation.
(F) Schematic of real-time place preference assay.
(G) ChR2 mice, but not eYFP controls, exhibit frequency-dependent preference for stimulation-paired compartment that reversed when contingencies changed.
(H) Schematic of CPP and hybrid RTPP/CPP procedure using bilateral stimulation. Memory was assessed in test 1 (no stimulation); surgical efficacy was assessed via RTPP in test 2.
(I) Pavlovian CeA→SNL stimulation did not elicit CPP in test 1 but robust RTPP was observed in test 2.
(J) Instrumental CeA→SNL stimulation induced a brief preference for the stimulation-paired chamber.
(K) Schematic of conditioned reinforcement procedure.
(L) ChR2 mice that received cue-stimulation pairings do not develop a preference for the active, cue-producing lever during the conditioned reinforcement test and were indistinguishable from controls.
(M) During the primary reinforcement test, ChR2 groups developed a preference for the active lever.
(N) ChR2 groups exhibited equivalently robust RTPP.
*$p < 0.05$; ***$p < 0.001$. Error bars indicate SEM.
See also Figure S2 and Table S1.

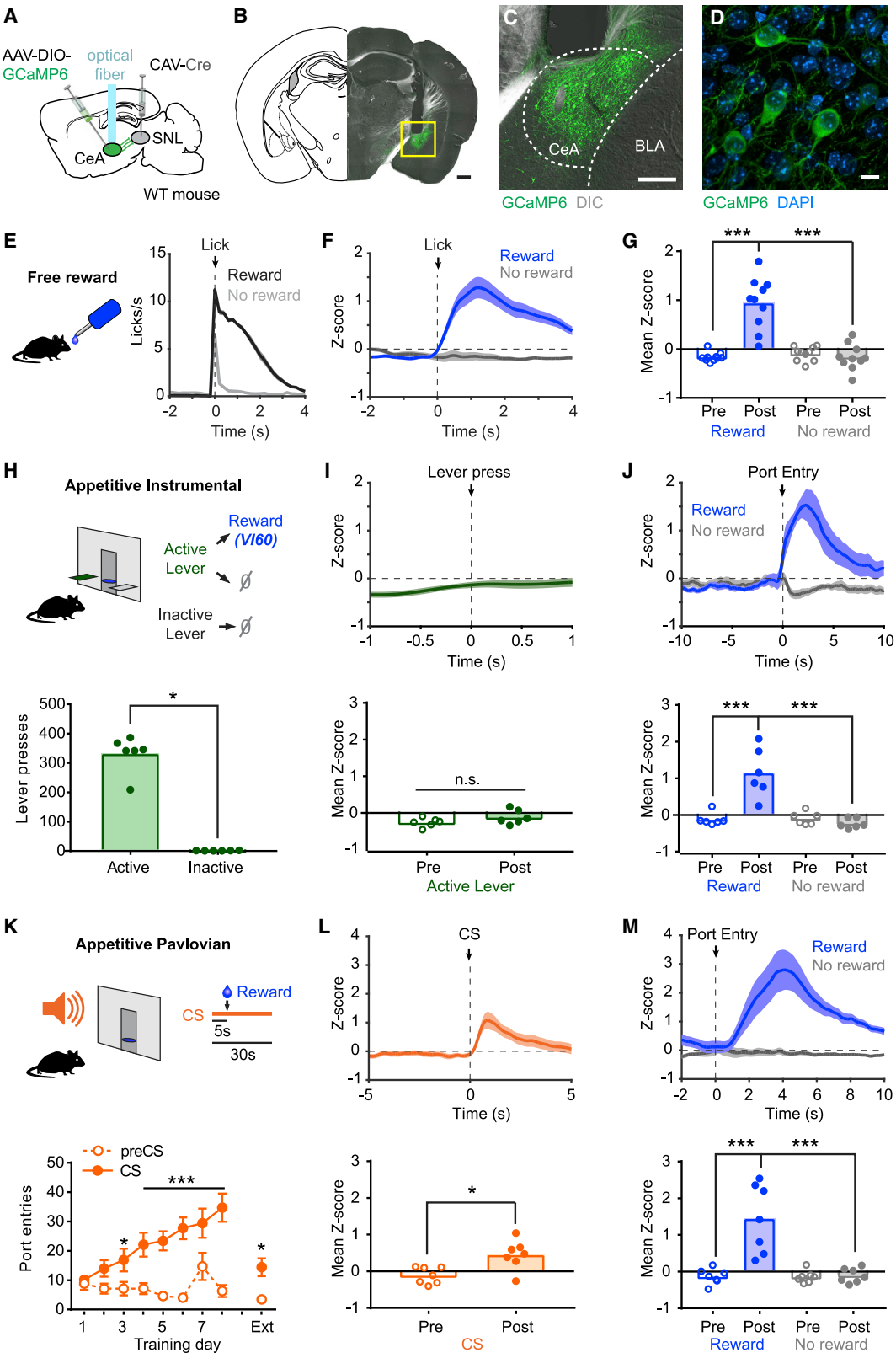

(legend on next page)

preference (CPP) assay where contextual stimuli are paired with a putative rewarding experience (Figure S2H). Surprisingly, in mice that had shown robust ICSS for CeA→SNL stimulation, the same manipulation failed to induce any CPP (Figure S2I; $p > 0.236$). To ensure that we could detect CPP, the same mice received a dose of cocaine, which produced clear preference for the drug-paired chamber (Figures S2J and S2K; $p < 0.001$). To test if the single-day optogenetic procedure was too short to induce CPP, we repeated the assay using an extended conditioning protocol (Figure 2H). However, 90 min of stimulation over 3 days was not sufficient to elicit CPP even in the first minutes of the test (Figure 2I; t test, first 5 min bin ChR2 versus eYFP $p = 0.0778$, trending toward aversion). Failure to elicit Pavlovian learning cannot be explained by ineffective CeA→SNL pathway activation, since the same animals exhibited robust RTPP (Figure 2I; $p < 0.001$).

CPP requires the effects of stimulation to be recalled at a later time, while ICSS and RTPP involve instant behavioral readouts with no memory demands. If the lack of CPP resulted from a memory failure, we predicted that the same memory failure should occur when the effects of instrumental manipulations were assessed later. To test this, we performed a 3-day RTPP experiment and assessed place preference 1 day later (Figure 2H). During the post-conditioning test (test 1), ChR2 mice exhibited a brief preference for the paired compartment in the absence of stimulation (Figure 2J; t test, first 5 min bin ChR2 versus eYFP $p = 0.0128$), indicating they remembered where they had received stimulation. As an additional control, we examined learning effects in a two-choice ICSS task using the same temporal parameters as our CPP procedure (Figure S2L). Mice acquired robust ICSS (Figure S2M; $p < 0.004$) and responded faster across days (Figure S2N; $p < 0.037$ on days 3–4), consistent with a learning effect. Furthermore, active nosepoke preference persisted in an extinction test (Figure S2O; $p = 0.003$). These results suggest that the lack of CPP cannot be explained by memory impairment.

CPP procedures measure the ability of primary rewards to confer incentive value to contextual stimuli experienced over minutes to hours. Sensory events can also acquire incentive value through predictive association with rewards on much shorter timescales. To assess whether CeA→SNL pathway activation supports Pavlovian learning about discrete stimuli, we used a conditioned reinforcement procedure (Figure 2K), a canonical test of a cue's incentive value (Taylor and Robbins, 1984). We paired a brief tone-light cue with CeA→SNL stimulation and asked if presentations of the cue alone would drive acquisition of a novel instrumental response (Figure 2K). Despite extensive training, during the conditioned reinforcement test, mice responded equivalently at the active (cue-producing) and inactive (control) lever (Figure 2L; $p > 0.687$). We confirmed that stimulation was effective by verifying that it supported ICSS (Figure 2M; $p < 0.014$) and RTPP (Figure 2N; $p < 0.001$). Collectively, these results demonstrate that the behavioral consequences of CeA→SNL pathway activation depend on the subject's degree of control over this experience. Optogenetic stimulation could readily reinforce simple actions, but the same manipulation in the same animals failed to confer incentive value to either contextual or discrete cues via passive Pavlovian pairing.

CeA→SNL Neurons Are Activated by Appetitive and Aversive Stimuli

Although CeA→SNL pathway activation had robust effects, it is unclear how the activity imposed in gain-of-function experiments relates to natural activity in CeA→SNL neurons. To address this, we expressed GCaMP6 in CeA→SNL neurons and measured population activity with fiber photometry (Lerner et al., 2015) (Figures 3A–3D, S3A, and S3B). We examined CeA→SNL neuron activity as mice consumed sucrose at a lickometer (Figure 3E). CeA→SNL neurons were robustly activated following rewarded, but not unrewarded, licks (Figures 3F and 3G; $p < 0.001$), indicating that CeA→SNL neurons are activated by natural rewards and not by movements required for licking. In an instrumental learning task where lever presses were reinforced on a variable interval (VI) 60-s schedule (Figure 3H), CeA→SNL neurons responded minimally to lever press (Figure 3I; $p = 0.0875$) but were strongly activated by sucrose (Figure 3J; $p < 0.001$). These results demonstrate that the activation patterns used in ICSS experiments mimic the direction and timing of natural neural activity during instrumental learning.

Figure 3. CeA→SNL Neurons Are Activated by Natural Rewards during Appetitive Learning

(A) Strategy for recording CeA→SNL neuron population activity.
(B) Representative histology (scale bar, 500 μm). Box shows area enlarged in (C).
(C) High-magnification view of CeA virus expression and fiber placement (scale bar, 250 μm).
(D) High-magnification view of GCaMP6-expressing CeA neurons (scale bar, 10 μm).
(E) Left: schematic of free reward task. Right: behavioral data (n = 10 mice) plotting lick rate for rewarded and unrewarded lick events.
(F) Group average neural response to rewarded and unrewarded licks.
(G) Mean *Z* score for a 2-s window before and after rewarded and unrewarded licks.
(H) Top: schematic of appetitive instrumental task. Bottom: behavioral data (n = 6 mice).
(I) Top: group average neural response to active lever press. Bottom: mean *Z* score during a 1-s window before and after active lever press.
(J) Top: group average neural response to rewarded and unrewarded port entries. Bottom: mean *Z* score during a 5-s window before and after port entry.
(K) Top: schematic of appetitive Pavlovian task. Bottom: port entries made during the 5 s immediately prior to cue onset (preCS) and the first 5 s of the cue (CS) plotted across training (n = 7 mice).
(L) Top: group average neural response to CS onset (training day 7). Bottom: mean *Z* score during the 5-s window before and after CS onset.
(M) Top: group average neural response to rewarded and unrewarded port entries (training day 7). Bottom: mean *Z* score during the 10-s window before and after port entry.
*$p < 0.05$; **$p < 0.01$; ***$p < 0.001$. Error bars or shaded regions indicate SEM.
See also Figures S3 and S8 and Table S1.

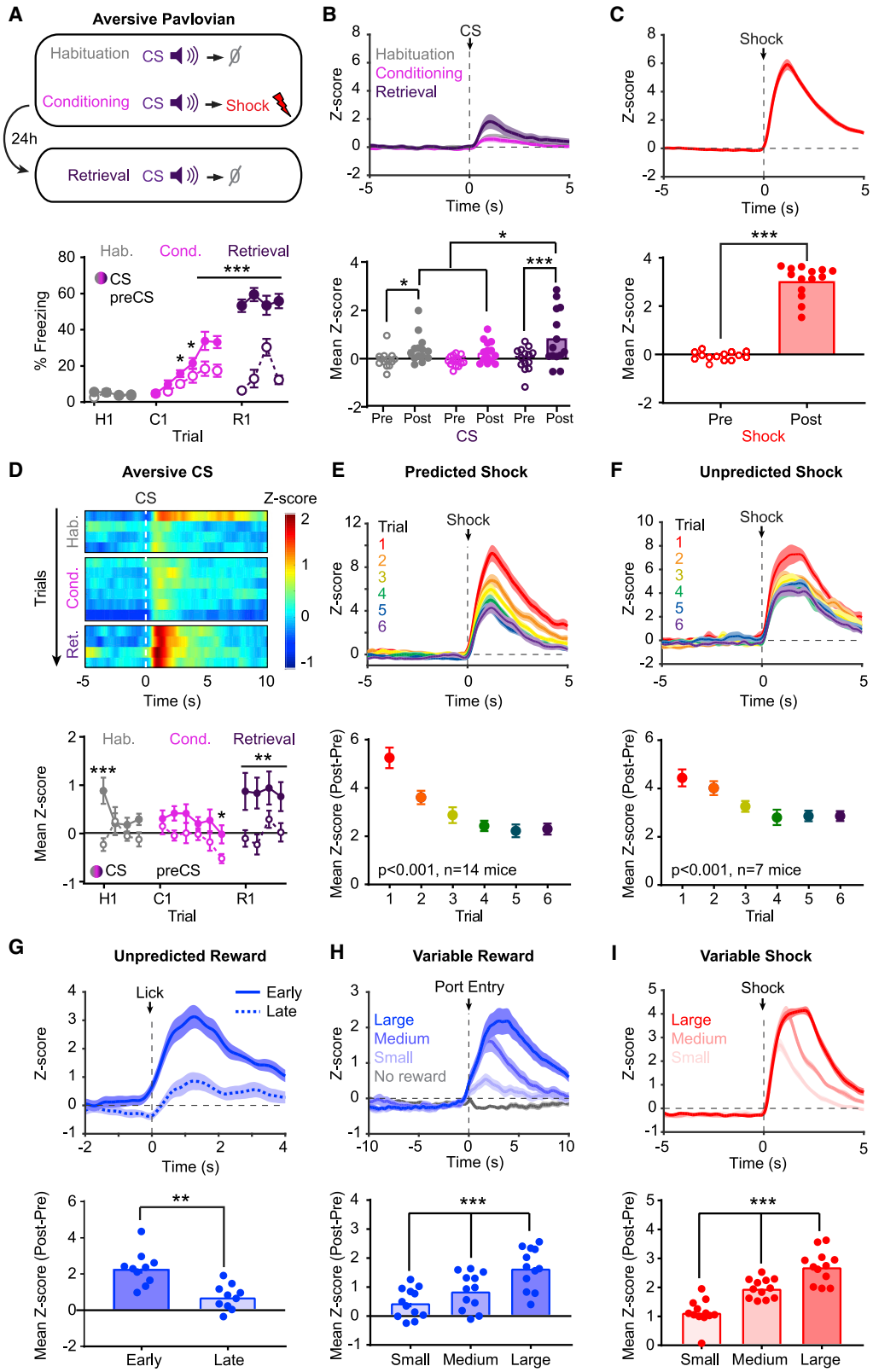

(legend on next page)

To determine how CeA→SNL neurons respond during appetitive Pavlovian learning, we trained mice to associate an auditory cue (conditioned stimulus [CS]) with sucrose (unconditioned stimulus [US]) (Figure 3K). Late in training on day 7, CeA→SNL neurons were moderately activated by the auditory CS (Figure 3L; $p = 0.035$) and more strongly activated by the US (Figure 3M; $p < 0.001$). The relative strength of CS and US signals remained consistent across training (Figures S3C and S3D).

Given the CeA's established role in learned aversive behaviors, we next examined whether CeA→SNL neurons also respond to stimuli that are not rewarding. We trained the same mice on an aversive Pavlovian association (i.e., fear conditioning) using a different auditory CS (Figure 4A). CeA→SNL neurons were activated by the novel cue during habituation trials and during the retrieval test the following day, but not during conditioning itself (Figure 4B, habituation $p = 0.049$, conditioning $p = 0.087$, retrieval $p < 0.001$). CeA→SNL neurons were more robustly activated by the shock US (Figure 4C; $p < 0.001$; Figure S3F), consistent with the relative magnitude of CS-US signals observed during appetitive training.

Activation by both appetitive and aversive stimuli indicates that, at the population level, CeA→SNL neurons encode a shared feature of rewarding and aversive events such as salience. If so, their activity should track changes in stimulus features that reflect salience, such as expectation and magnitude. To test this hypothesis, we examined CS-evoked CeA→SNL neural activity across trials during aversive Pavlovian learning, predicting that the CS would have perceptual salience on the first habituation trial due to its novelty and acquire learned salience through association with the aversive US. Consistent with these predictions, the CS evoked a prominent response on the first habituation trial that declined quickly (Figure 4D; $p < 0.001$), while sustained responses were observed across retrieval trials (Figure 4D; $p < 0.01$). Notably, potentiated CS responses lagged behind behavioral evidence of learning during conditioning (CS freezing: Figure 4A; main effect of trial $p < 0.001$; CS Z score: Figure 4D; no effect of trial, $p = 0.326$). We next evaluated the neural response to shocks across successive trials, predicting that shocks should be more salient on earlier trials when they were least expected. Indeed, we found a strong relationship between the magnitude of shock responses and trial number (Figure 4E; $p < 0.001$). However, during conditioning, salience is confounded by learning as the US becomes less surprising precisely because learning is occurring. To determine whether CeA→SNL neuron responses also decrease with successive presentations of the same aversive US in the absence of learned predictions, we delivered unsignaled shocks in a separate session. Again, neural shock response decreased with successive trials (Figure 4F; $p < 0.001$). To address if responses to appetitive USs follow a similar pattern, we reexamined activity during early and late trials of a free reward session (Figure 3E) and found that neural responses to sucrose were indeed larger on earlier trials (Figure 4G; $p = 0.002$).

We next asked whether CeA→SNL activity would track stimulus magnitude, reasoning that larger stimuli should be more salient. Population activity robustly tracked stimulus magnitude when unpredicted rewards or shocks of varying sizes were delivered in separate sessions to the same mice (Figures 4H and 4I; $p < 0.001$). Finally, the omission of an expected US is also a salient event capable of supporting new learning that requires the CeA (Holland and Kenmuir, 2005). Therefore, we examined neural responses at the expected time of US delivery during the first extinction/retrieval trial following appetitive or aversive Pavlovian conditioning. We did not observe changes in population activity in response to reward or shock omission (Figures S3E and S3G; $p > 0.447$), suggesting that reward omission responses observed in rat CeA (Calu et al., 2010) likely arise from other CeA populations.

CeA→SNL Projections Are Necessary for Appetitive and Aversive Learning

We next asked whether the activity patterns we observed were required for successful behavioral performance. To suppress CeA→SNL activity, we injected an AAV encoding NpHR3.0 or eYFP into the CeA in wild-type mice and implanted an optical fiber above SNL (Figures 5A, S4A, and S4B). We trained mice to lever press for sucrose on a VI60 schedule (Figure 5B). Optogenetic inhibition coincided with reward consumption to suppress the strongest neural signals observed in photometry experiments (Figure 3J). Inhibiting CeA→SNL neurons reduced the

Figure 4. CeA→SNL Neurons Are Activated by Noxious Stimuli during Aversive Learning

(A) Top: schematic of aversive Pavlovian task. Bottom: behavioral data (n = 14 mice).

(B) Top: group average neural response to cue onset during habituation, conditioning, and retrieval. Bottom: mean Z score during the 5-s window before and after cue onset.

(C) Top: group average neural response to shock. Bottom: mean GCaMP6 Z score during the 5-s window before and after shock.

(D) Top: heatmap of group average CS responses across habituation, conditioning, and retrieval trials. Bottom: mean Z score during the 5-s window before and after cue onset for each trial.

(E) Top: group average neural response to shock across 6 fear conditioning trials (n = 14 mice). Bottom: difference in post-shock versus pre-shock mean Z scores (5-s window).

(F) Top: group average neural response to shock onset for 6 unpredicted shock trials (n = 7 mice). Bottom: difference in post-shock versus pre-shock mean Z scores (5-s window).

(G) Top: group average neural response to rewarded licks for early (first 5/50) and late (last 5/50) trials within a single session (n = 10 mice). Bottom: difference in post-reward versus pre-reward mean Z scores (2-s window).

(H) Top: group average neural response to port entry (n = 12 mice) in a session where unpredicted rewards of variable volume are delivered. Bottom: difference in post-reward versus pre-reward mean Z scores (10-s window).

(I) Top: group average neural response (n = 12 mice) to shock in a session where unexpected shocks of variable duration are delivered in interleaved trials. Bottom: difference in post-shock versus pre-shock mean Z scores (5-s window).

*$p < 0.05$; **$p < 0.01$; ***$p < 0.001$. Error bars or shaded regions indicate SEM.

See also Figures S3 and S8 and Table S1.

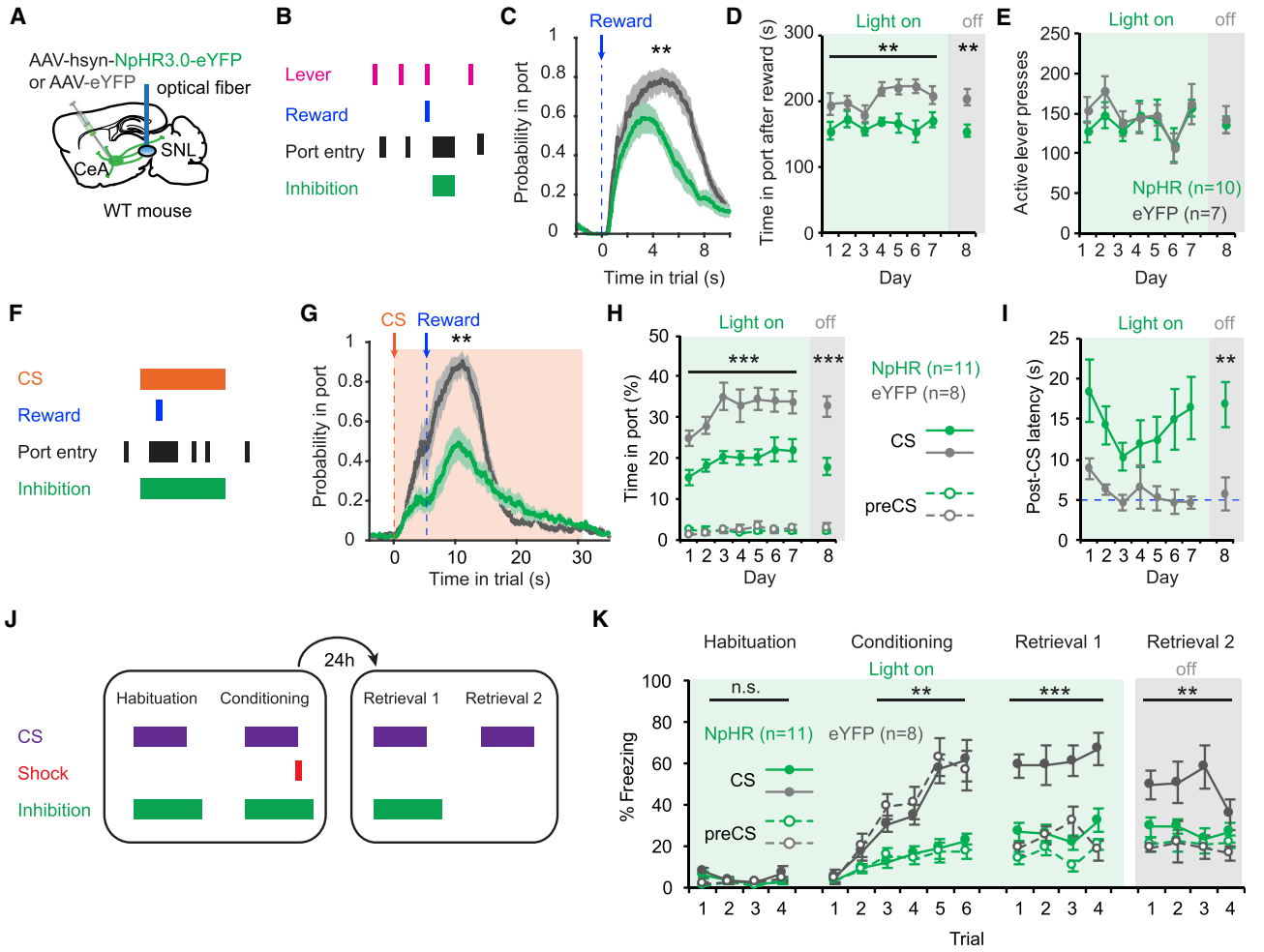

Figure 5. CeA→SNL Neurons Are Necessary for Appetitive and Aversive Learning

(A) Strategy for inhibiting CeA→SNL projections.

(B) Trial structure for appetitive instrumental inhibition experiments. Inhibition was timed to suppress neural activity during reward consumption.

(C) Data from a single session late in training. Reward seeking was disrupted in NpHR mice.

(D) NpHR mice spent less time in the reward port in the 10 s following reward delivery and this effect persisted when light was turned off.

(E) Inhibition during reward consumption did not affect acquisition or performance of the instrumental response.

(F) Trial structure for appetitive Pavlovian inhibition experiments. Inhibition was timed to suppress neural activity during the cue and reward.

(G) Data from single session late in training. Inhibition impaired conditioned reward seeking in NpHR mice.

(H) NpHR mice spent less time in the reward port during the CS across training days and this effect persisted when light was turned off.

(I) eYFP mice entered reward port more quickly after the CS, with response latencies anticipating reward delivery (dashed blue line) on days 3–7. NpHR mice did not show this relationship. With light off, eYFP mice continued to respond to the CS more quickly than the NpHR group.

(J) Trial structure for aversive Pavlovian inhibition experiments. Inhibition was timed to suppress neural activity during the CS and shock.

(K) NpHR mice exhibited reduced freezing during conditioning (retrieval 1), and this difference persisted in retrieval 2 trials when the light was off.

**p < 0.01; ***p < 0.001. Error bars or shaded regions indicate SEM.

See also Figure S4 and Table S1.

probability of port entry following reward delivery (Figure 5C; p = 0.004) and the total time in the port following reward (Figure 5D; p = 0.01). This effect was stable across training days and persisted during a probe session where the light was turned off (Figure 5D; p = 0.004). In contrast to the durable changes to reward-seeking behavior, optogenetic inhibition had no effect on the acquisition or performance of the instrumental response itself, as NpHR- and eYFP-mice responded similarly on the active lever (Figure 5E; p > 0.612).

Because we observed neural activation to the CS and US during appetitive Pavlovian learning (Figures 3L and 3M), we also inhibited CeA→SNL terminals while pairing an auditory CS with sucrose reward (Figure 5F). This inhibition strongly reduced the probability of port entry during the CS (Figure 5G; p = 0.0067), with NpHR mice spending less time in the reward port during the CS across all training days (Figure 5H; p < 0.001). While control mice learned to respond more quickly to the CS to anticipate reward delivery (Figure 5I; p =

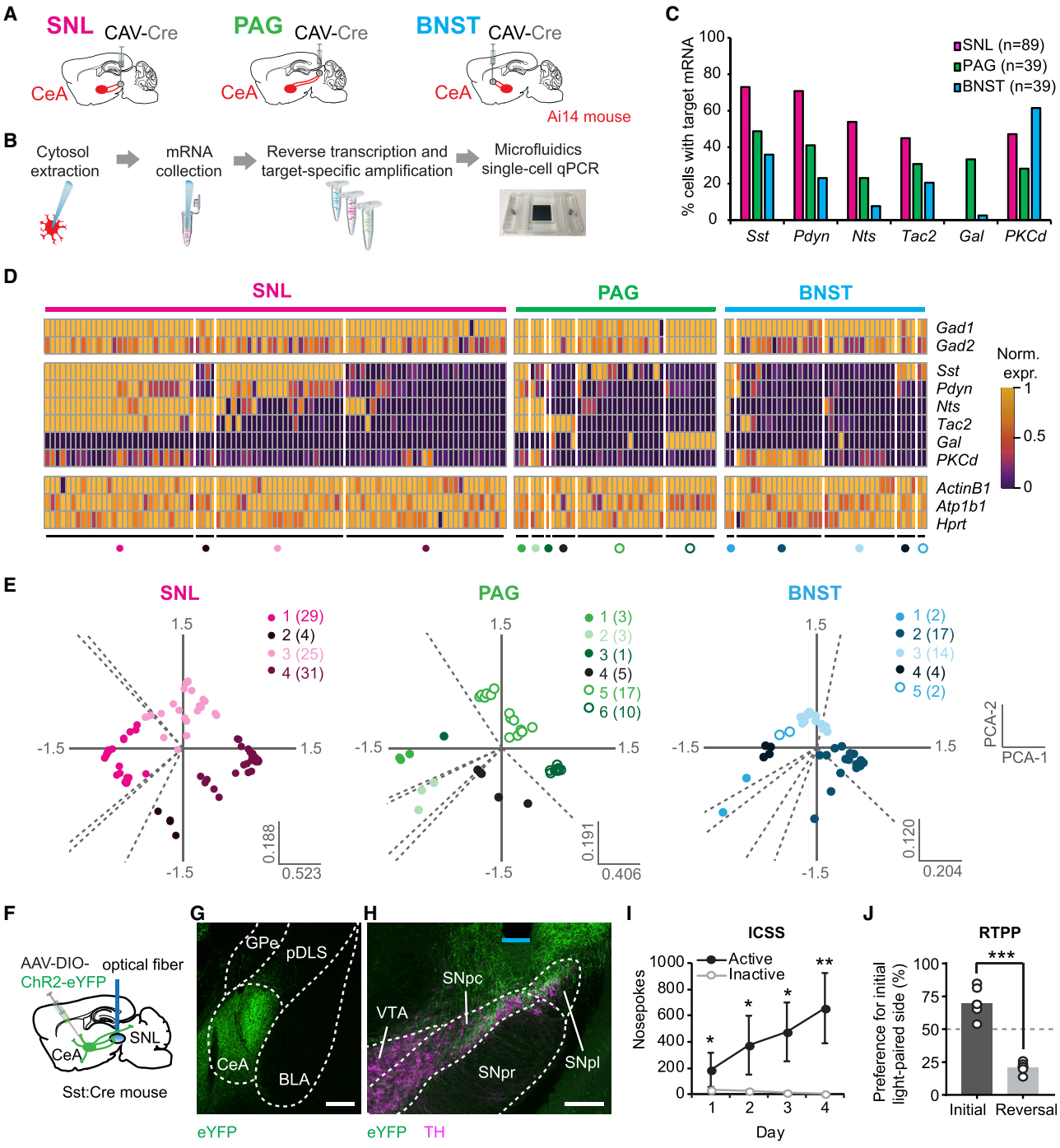

Figure 6. Genetic Profile of Projection-Defined CeA Neurons

(A) Strategy to label projection-defined CeA populations.

(B) Schematic of single-cell transcriptomics workflow.

(C) Summary data for somatostatin (*Sst*), prodynorphin (*Pdyn*), neurotensin (*Nts*), tachykinin2 (*Tac2*), galanin (*Gal*), and protein kinase C-delta (*PKCd*) (n = 167 cells from 8 mice).

(D) Heatmap representation of normalized gene expression for all cells, grouped by projection target.

(E) Principal-component analysis (PCA) of gene expression relationships within each projector population. Numbers in parentheses indicate number of cells in each cluster.

(F) Strategy for activating *Sst*$^{+}$ CeA→SNL projections.

(G) Representative CeA virus expression (scale bar, 250 μm).

(legend continued on next page)

0.003), NpHR mice did not ($p = 0.085$). Behavioral deficits persisted during a light-off probe test, where NpHR mice exhibited reduced reward-seeking behavior during the CS (Figure 5H; $p < 0.001$) and slower response latencies (Figure 5I; $p = 0.003$).

The suppression of reward seeking induced by CeA→SNL inhibition could be the result of impaired learning, generation of a negative value signal, or decreased motivation for sucrose. To distinguish between these possibilities, we first asked if CeA→SNL inhibition led to place avoidance in a real-time place preference task. NpHR mice neither avoided nor preferred the side of the chamber paired with inhibition (Figure S4C; $p = 0.717$). We then asked if CeA→SNL inhibition altered intrinsic motivation to consume sucrose. Mice freely consumed sucrose from a lickometer in the presence and absence of lick-triggered inhibition. The sucrose consumed and number of licks were unaffected by inhibition (Figure S4D; no group × phase interaction, $p > 0.38$). Taken together, these data suggest that the behavioral deficits we observed in appetitive tasks are not a consequence of a place aversion to the reward port or reduced motivation to consume sucrose. Instead, our results are best explained as failure to learn optimal response timing dictated by associative relationships.

Finally, we asked if inhibiting CeA→SNL neurons would affect aversive Pavlovian learning, since salience signals should modulate behaviors elicited by positive and negative stimuli. We trained the same mice on a fear-conditioning task using a distinct auditory CS and applied inhibition during the CS and shock (Figure 5J) to suppress previously observed neural activity (Figures 4B and 4C). This manipulation dramatically impaired acquisition of the CS-US association; NpHR mice froze less than eYFP mice during the CS (Figure 5K, conditioning and retrieval 1; $p < 0.001$), and this effect persisted when the light was turned off (Figure 5K, retrieval 2; $p = 0.005$). Importantly, inhibition did not alter locomotion in an open field arena (Figure S4E; $p > 0.303$), indicating that changes in conditioned freezing were not a secondary consequence of altered movement. Thus, our data demonstrate that CeA→SNL signals are necessary for appetitive and aversive Pavlovian learning, as well as appropriately timed reward seeking in instrumental tasks.

Genetic Profile of CeA→SNL Neurons

Genetically distinct CeA subpopulations have been linked to specific functional roles (Fadok et al., 2018; Li, 2019). To assess if CeA→SNL neurons constitute a unique genetic population within the CeA, we injected a retrograde CAV-Cre virus into the SNL of Ai14 Cre-reporter mice to label CeA→SNL neurons and performed single-cell quantitative PCR (qPCR) following cytosol extraction (Fuccillo et al., 2015). For comparison, we examined periaqueductal gray (PAG) and bed nucleus of the stria terminalis (BNST)-projecting populations, which have been implicated in behavioral responses to discrete and sustained threats, respectively (Tovote et al., 2016; Asok et al., 2018) (Figures 6A, 6B, and S5A). For each cell ($n = 167$), we quantified mRNA expression levels of six target genes expressed in CeA: somatostatin (*Sst*), prodynorphin (*Pdyn*), neurotensin (*Nts*), tachykinin2 (*Tac2*), galanin (*Gal*), and protein kinase C-delta (*PKCd*) (Figure 6C). With the exception of neurons expressing *Gal*, which almost exclusively projected to PAG, all transcripts were represented within each projector population, albeit at different levels. *Sst*, *Pdyn*, *Nts*, and *Tac2* were preferentially expressed in CeA→SNL neurons while *Gal* and *PKCd* were preferentially expressed in CeA→PAG and CeA→BNST neurons, respectively. These results suggest that CeA→SNL neurons overlap with genetically defined CeA populations previously implicated in aversive learning (*Sst*, *PKCd*, and *Tac2*) (Andero et al., 2016; Li, 2019; Fadok et al., 2018) as well as populations that support self-stimulation (*Sst*, *Nts*, and *Tac2*) (Kim et al., 2017).

To more comprehensively identify patterns of gene expression within each projector population, we used principal-component analysis (Figures 6D and 6E). This revealed four, six, and five clusters within CeA→SNL, CeA→PAG and CeA→BNST neuron populations, respectively. CeA→SNL neurons tended to co-express *Sst*, *Pdyn*, *Nts*, and *Tac2* with variable levels of *PKCd* and no *Gal*. An independent principal-component analysis on data from all projector populations combined (Figures S5B–S5E) revealed that cells co-expressing these four genes again emerge as a unique cluster and ~75% of cells in this cluster are CeA→SNL neurons. Thus, while we did not find a genetic signature that selectively defined CeA→SNL neurons, there appear to be subpopulations of CeA→SNL neurons with distinct gene expression profiles.

CeA Sst^+ neurons have been implicated in both appetitive and defensive behaviors (Li, 2019). Given that CeA→SNL neurons are activated by both appetitive and aversive stimuli and the majority (>70%) of these cells are Sst^+, we asked if optogenetic activation of CeA Sst^+ axon terminals in SNL would result in a similar behavioral phenotype as our pan-neuronal, projection-specific manipulation (Figure 2). We injected a Cre-dependent ChR2 virus into the CeA of *Sst*:Cre mice (Taniguchi et al., 2011) and implanted an optical fiber above axon terminals in the SNL (Figures 6F–6H and S5F). We observed robust ICSS (Figure 6I; $p < 0.023$) as well as RTPP (Figure 6J; $p < 0.001$) for 20-Hz optical stimulation, indicating that activation of Sst^+ CeA→SNL projections is sufficient to reinforce instrumental associations. Importantly, the increased specificity afforded by genetic targeting resulted in minimal virus expression in structures adjacent to the CeA or axon terminals ventral to SNL, providing an anatomical cross-check on our previous results.

Inhibitory CeA Inputs Preferentially Contact SNL GABA Neurons

The SNpc and SNpl are primarily composed of DA and GABA neurons, with the proportion of DA neurons decreasing laterally. To determine which population receives CeA input, we used cell-type-specific, monosynaptic rabies virus tracing

(H) Representative midbrain virus expression and fiber placement. Blue line indicates fiber tip (scale bar, 250 μm).
(I) Stimulation of Sst^+ CeA→SNL projections drives positive reinforcement in a two-choice ICSS task ($n = 8$ mice).
(J) Stimulation also supported RTPP that reversed within the same session ($n = 8$ mice).
*$p < 0.05$; **$p < 0.01$; ***$p < 0.001$. Error bars indicate SEM.
See also Figure S5 and Table S1.

(Wickersham et al., 2007) in DAT:Cre (Bäckman et al., 2006) or Vgat:Cre (Vong et al., 2011) mice to target DA or GABA neurons, respectively (Figure 7A; Figures 7B and 7C, left). AAVs encoding a Cre-dependent avian viral receptor (TVA) fused to mCherry (TC) and a Cre-dependent rabies glycoprotein (G) were injected into the SNL. 2 weeks later, an EnvA-pseudotyped, G-deleted rabies virus expressing GFP was injected into the same location, and animals were sacrificed after 5 days. We intentionally used a TVA variant (TC^{66T}) with reduced transduction efficiency that enables detection of both local and long-range connections (Miyamichi et al., 2013). Within the SNL, we found local GFP^+/TH^- (tyrosine hydroxylase; presumed GABAergic) inputs to DA neurons in DAT:Cre mice (Figures S6A–S6C). Within the CeA, we found GFP^+ input neurons in both DAT:Cre and Vgat:-Cre mice (Figures 7B and 7C, right), demonstrating that both SNL cell types are targeted by long-range CeA projections. GFP^+ cells were not found in control experiments where AAVs were omitted (Figures S6D–S6G).

To assess the functional strength of these connections, we expressed ChR2 in the CeA and Cre-dependent tdTomato in the SNL of DAT:Cre or Vgat:Cre mice and performed whole-cell recordings from labeled DA and GABA cells in acute SNL brain slices (Figures 7D–7F and S6L). Monosynaptic CeA→SNL connections were isolated by bath application of tetrodotoxin (TTX) and 4-aminopyridine (4-AP) (Tritsch et al., 2012). Consistent with rabies-tracing results, activation of CeA axons generated inhibitory postsynaptic currents (IPSCs) in both DA and GABA neurons within the SNL. However, the functional strength of this connectivity was significantly larger in GABA neurons. A larger proportion of GABA neurons received CeA connections (Figure 7G), and IPSC amplitudes were higher in connected GABA cells than in connected DA cells (Figures 7H and 7I; Vgat 706 ± 121 pA, DAT 282 ± 57 pA, $p = 0.039$). Importantly, this pattern was replicated when DA and GABA neurons were recorded in the same brain slice (Figures S6H–S6L). Light-evoked currents were blocked by the $GABA_A$ receptor antagonist picrotoxin (Figure 7H), confirming the inhibitory nature of CeA connections.

The preferential connectivity of inhibitory CeA inputs onto SNL GABA neurons is consistent with the hypothesis that CeA→SNL neurons activate SNL DA neurons via disinhibition. To further evaluate this possibility, we injected a Cre-dependent ChR2 virus into the SNL of Vgat:Cre mice crossed with a Th:GFP reporter (Sawamoto et al., 2001) (Figures 7J, 7K, and S6M) and looked for inhibitory connections between local GABA neurons and GFP^+ SNL DA neurons. DA cell identity was confirmed post hoc using TH immunohistochemistry, as fluorophore expression in TH^- cells has been reported in this line (Lammel et al., 2015). Light-evoked IPSCs were observed in all SNL DA neurons ($n = 6$; Figures 7L and 7M; mean IPSC 456 ± 128 pA). These data indicate that CeA inputs have the potential to influence SNL neural activity in multiple ways by directly inhibiting SNL GABA or DA neurons and/or activating SNL DA neurons via disinhibition.

SNL DA Neurons Are Activated by Appetitive and Aversive Stimuli

Since CeA→SNL neurons may disinhibit SNL DA neurons, we hypothesized that SNL DA neurons should exhibit similar excitatory responses to salient events. To test this prediction, we expressed GCaMP6 in the SNL of DAT:Cre mice (Figures 8A, 8B, S7A, and S7B) to measure SNL DA neuron activity. Consistent with our hypothesis, we found many similarities in the response profiles of CeA→SNL and SNL DA neurons to salient stimuli. During appetitive instrumental learning (Figure 8C), SNL DA neurons showed small increases in activity following lever press (Figure 8D; $p = 0.004$) and larger activation to port entries when sucrose was present (Figure 8E; $p < 0.001$). During appetitive Pavlovian learning (Figure 8F), SNL DA neurons were activated by the sucrose-predictive CS (Figure 8G; $p < 0.001$) and sucrose itself (Figure 8H; $p < 0.001$). During aversive Pavlovian conditioning (Figure 8I), SNL DA neurons encoded both perceptual salience of the novel stimulus during habituation as well as learned salience during retrieval (Figure 8J; $p < 0.001$). SNL DA neurons were also robustly activated by the shock US (Figure 8K; $p < 0.001$) and US responses were larger than CS responses (Figure S7F). SNL DA neurons were weakly inhibited by reward omission (Figure S7E; $p = 0.029$) and unaffected by shock omission (Figure S7G; $p = 0.382$). The lack of prominent US omission responses replicates findings from primate single-unit recording studies (Matsumoto and Hikosaka, 2009) and indicates that CeA→SNL and SNL DA salience signals are limited to the presence, but not unexpected absence, of motivationally significant stimuli.

SNL DA neurons differed from CeA→SNL neurons in the strength and speed of CS responses. Late in appetitive Pavlovian training, CeA→SNL neurons had weak CS and comparatively strong US responses (Figure S4C). In contrast, SNL DA neurons showed the opposite relationship, with strong CS and comparatively weaker US signals (Figures S7C and S7D). During aversive Pavlovian training, CeA→SNL neurons were slow to encode the learned salience of the aversive CS (Figure 4D). In contrast, SNL DA CS responses emerged rapidly on the same timescale as behavioral discrimination (Figure 8L); both neural and behavioral potentiation was evident by conditioning trial 3 (trial C3 versus C1: CS Z score $p < 0.001$; Figure 8L; CS freezing $p < 0.001$; Figure 8I). Thus, while some differences between CeA→SNL neuron and SNL DA neuron activity were evident, overall, there was substantial similarity in the salience signals encoded by these populations (Figure S8).

DISCUSSION

CeA Circuits and Emotion

Elucidating the neural basis of emotional behavior has clear therapeutic relevance, as emotional dysregulation is a hallmark of many forms of mental illness (Sheppes et al., 2015). Contemporary psychological theories postulate that core affect, a crucial component of human emotion, can be described by the orthogonal dimensions of pleasure-displeasure (valence) and activation-deactivation (arousal) (Russell, 2003), offering a useful framework to study emotion in animals. Thus, identifying neural circuit elements that support adaptive responses to positive and negative stimuli and determining the extent to which these are segregated or overlapping will be important to understand how emotions are constructed in health and disease.

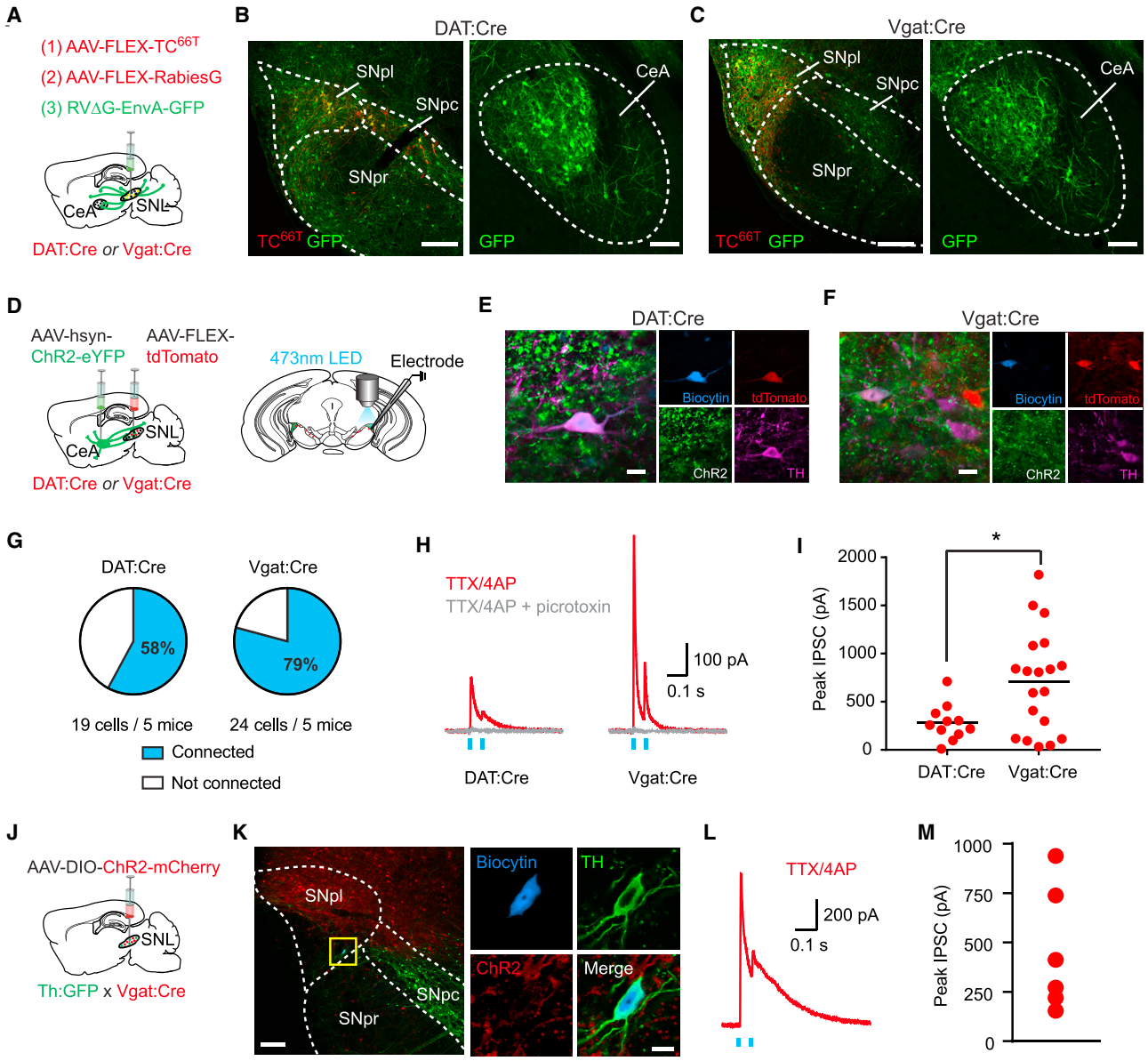

Figure 7. CeA Inputs Preferentially Target SNL GABA Neurons

(A) Injection strategy for cell-type-specific monosynaptic retrograde tracing.
(B) Left: representative histology of SNL injection site in DAT:Cre mouse. Right: GFP$^+$ input cells in CeA (scale bar, 200 μm/100 μm).
(C) As in (B), but for a Vgat:Cre mouse.
(D) Injection strategy for CeA→SNL synaptic connectivity experiments and schematic of recording configuration.
(E) Example recorded DA neuron showing co-localization of biocytin, tdTomato, TH, and ChR2 (scale bar, 10 μm).
(F) As in (E), but for a GABA neuron (scale bar, 10 μm).
(G) Percentage of DA and GABA neurons receiving monosynaptic CeA input.
(H) Sample light-evoked IPSCs, which were blocked by picrotoxin.
(I) Peak IPSC amplitudes for all connected cells. *$p < 0.05$.
(J) Injection strategy for intra-SNL synaptic connectivity experiments.
(K) Representative histology. Box shows location of recorded cell. Right: recorded cell at higher magnification (scale bars, 100 μm/10 μm).
(L) Light-evoked IPSC from the SNL DA neuron shown in (K).
(M) Peak IPSC amplitudes for all cells (six out of six connected from two mice).
See also Figure S6 and Table S1.

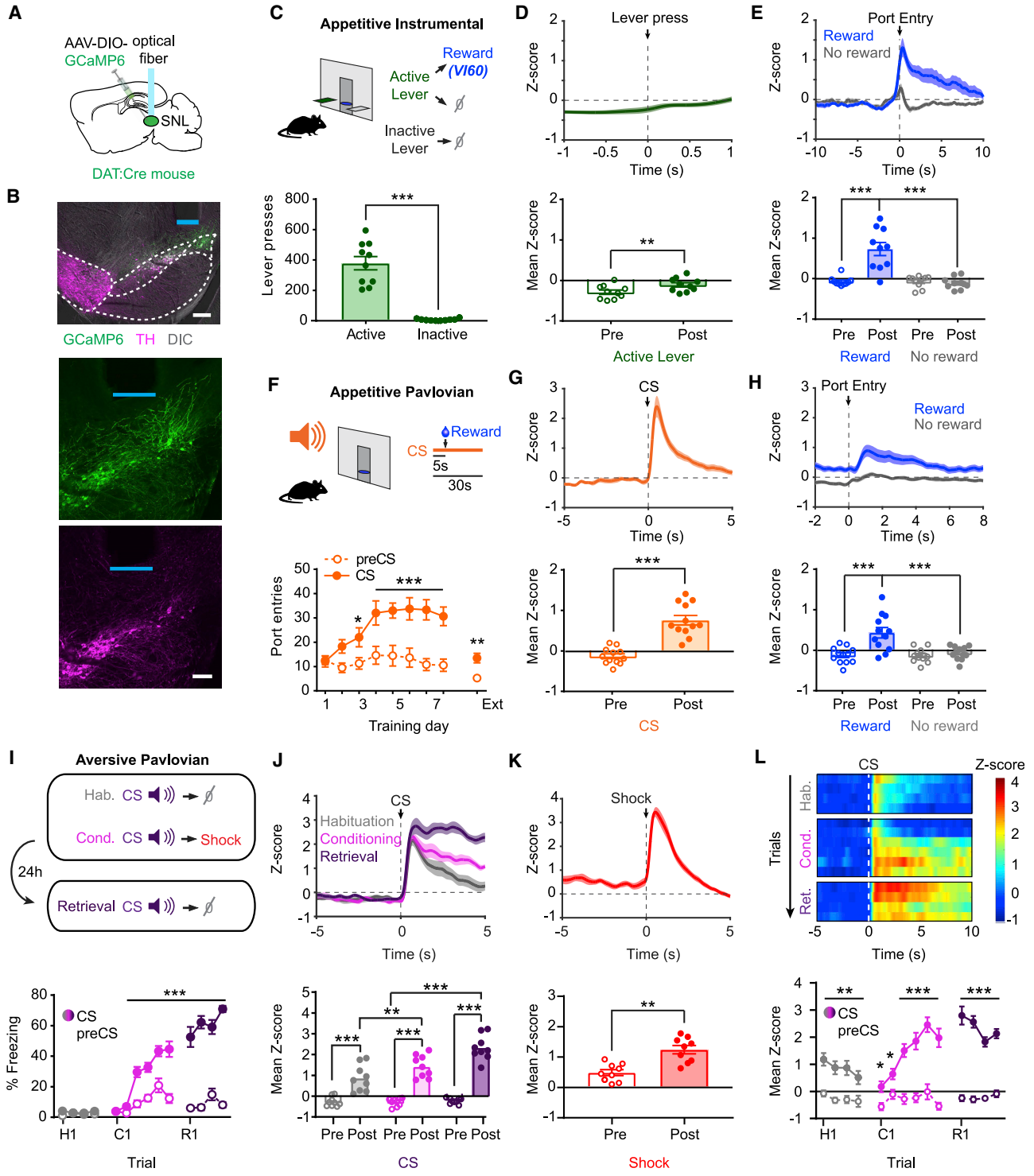

Figure 8. SNL DA Neurons Are Activated by Appetitive and Aversive Stimuli

(A) Strategy for recording population activity of SNL DA neurons.

(B) Representative GCaMP6 expression and optical fiber placement. Blue line indicates fiber tip (scale bar, 200 μm/100 μm).

(C) Top: schematic of appetitive instrumental task. Bottom: behavioral data (n = 10 mice).

(D) Top: group average neural response to active lever press. Bottom: mean *Z* score during the 1-s window before and after the active lever press.

(E) Top: group average neural response to rewarded and unrewarded port entries. Bottom: mean *Z* score during the 5-s window before and after port entry.

(legend continued on next page)

Typically, CeA studies focus on aversive learning, leading to conclusions about neural substrates "for fear" without assessing alternative behaviors. Here, we evaluated CeA→SNL projections using both appetitive and aversive learning tasks. We found that CeA→SNL neurons are activated by positive and negative stimuli during natural behavior and are essential for mounting an appropriate response to both events. The population-level signals we observed are compatible with distinct scenarios at the single-cell level; individual CeA→SNL neurons could respond similarly to appetitive and aversive stimuli (homogeneous salience), or separate populations could encode these events (heterogeneous valence). Although we could not definitively disambiguate these possibilities, several lines of evidence support our hypothesis that CeA→SNL neurons homogenously encode salience. First, single-unit recording studies have identified salience-encoding neurons in the CeA (Shabel and Janak, 2009). Second, stimulation of intermingled populations of CeA→SNL neurons with opposing valence would be expected to have net neutral valence or favor the dominant group (likely aversive since shock elicited the strongest neural response, which is consistent with the salience asymmetry between positive and negative stimuli). Instead, this manipulation produced homogeneous positive reinforcement. While it is not clear why a salience signal would serve to reinforce instrumental responding, intense sensory stimulation can be actively sought under some circumstances (Suarez, 2012). Third, the observed neural dynamics are most consistent with salience signaling; shock responses decreased across trials, while the negative value of painful shocks should have held constant. Furthermore, the aversive CS elicited a strong neural response the first time it was presented, at a time when it held salience through novelty but had not yet acquired negative value. Finally, this interpretation is most consistent with prior lesion disconnection studies in rats that identified a role for CeA→SNL interactions in salience-related attentional processes (Han et al., 1997; Lee et al., 2005, 2006).

We primarily used efferent connectivity to SNL as a means to parse multifunctional CeA circuits. Genetic identity is another important feature that contributes to functional selectivity (Fadok et al., 2018; Li, 2019). Our data suggest that the relationship between these variables is complex, and combinations of these and other factors may define more nuanced cellular identities that delineate functionally relevant CeA subpopulations. *Sst* proved to be the best genetic marker for CeA→SNL neurons, and our results comport with studies demonstrating *Sst*+ neurons are necessary for fear conditioning (Li et al., 2013), promote passive defensive behaviors (Yu et al., 2016; Fadok et al., 2017) and support self-stimulation (Kim et al., 2017). Furthermore, CeA→SNL neurons were activated by the aversive CS during retrieval, in line with previous findings that Sst^{+} neurons correspond to "CeL-on" neurons (Ciocchi et al., 2010; Yu et al., 2016; Fadok et al., 2017). Neurons expressing *PKCd*, a marker that labeled ~50% of CeA→SNL cells (some of which also expressed *Sst*), exhibit expectation-modulated shock responses (Yu et al., 2017), in line with our observation that CeA→SNL shock responses decreased across trials.

Distinct and Complementary Amygdala Connections to Heterogeneous Mesostriatal Circuits

Amygdala and mesostriatal subregions are increasingly appreciated to make differential contributions to Pavlovian and instrumental learning. Our finding that activation of CeA→SNL projections fails to support CPP or conditioned reinforcement is consistent with the hypothesis that BLA/VTA→NAc, but not CeA→SNL→DLS, circuits confer incentive properties to previously neutral stimuli via Pavlovian learning. This hypothesis is supported by demonstrations that CPP for natural rewards depends on BLA and NAc, but not DLS (Everitt et al., 1991), and that conditioned reinforcement is selectively modulated by DA manipulations within the NAc, but not dorsal/caudal striatum (Taylor and Robbins, 1986; Kelley and Delfs, 1991), and requires an intact BLA, but not CeA (Cador et al., 1989; Robledo et al., 1996). Furthermore, optogenetic VTA, but not SNc, DA neuron activation drives conditioned reinforcement (Saunders et al., 2018) and unblocks learning (Keiflin et al., 2019) when paired with Pavlovian cues in spite of the fact that both manipulations generate primary reinforcement, demonstrating medial-to-lateral functional differences in the ability of DA neurons to drive Pavlovian associations that rely on incentive value signals.

Theoretical accounts of instrumental learning differentiate between goal-directed and habitual responding, and distinct amygdala and mesostriatal circuits are thought to implement these processes (Balleine and O'Doherty, 2010). Goal-directed learning draws on an internal model of the world that incorporates specific stimulus features, including value, while motor programs are implemented without regard for the outcome they will produce in habit learning. We found that stimulation of CeA→SNL neurons could readily reinforce voluntary actions,

(F) Top: schematic of appetitive Pavlovian task. Bottom: port entries made during the 5 s prior to cue onset (preCS) and the first 5 s of the cue (CS) are plotted across training days (n = 12 mice).
(G) Top: group average neural response to CS onset on training day 7. Bottom: mean *Z* score during the 5-s window before and after CS onset, prior to reward delivery.
(H) Top: group average neural response to rewarded and unrewarded port entries on training day 7. Bottom: mean *Z* score during the 10-s window before and after port entry
(I) Behavioral data from aversive Pavlovian task (n = 9 mice).
(J) Top: group average neural response to cue onset during habituation and conditioning. Bottom: mean *Z* score during the 5-s window before and after cue onset.
(K) Top: group average neural response to shock. Bottom: mean *Z* score during the 5-s window before and after shock.
(L) Top: heatmap of group average CS responses across habituation, conditioning, and retrieval trials. Bottom: mean *Z* score during the 5-s window before/after cue onset across all trials.
*$p < 0.05$; **$p < 0.01$; ***$p < 0.001$. Error bars or shaded regions indicate SEM.
See also Figures S7 and S8 and Table S1.

but inhibition of CeA→SNL reward signals was not required for instrumental performance following moderate training, when performance was likely goal directed. Given that interactions between CeA and DLS, which are directly linked by SNL, have been implicated in habitual behaviors (Lingawi and Balleine, 2012; Murray et al., 2015), future studies should evaluate the contribution of CeA→SNL connections to instrumental performance after extended training.

To begin to determine the postsynaptic mechanisms that mediate information flow between the CeA and SNL, we assessed CeA connectivity with specific midbrain cell types using cell-type-specific transsynaptic tracing and *ex vivo* recordings. We found that CeA inputs target GABA and DA neurons in the SNL but preferentially inhibit GABA cells. Future work should address whether these represent parallel afferent pathways subject to independent regulation or instead arise from the same cells and clarify the net effect of suppressing CeA signals on DA and GABA neural activity *in vivo*. Systematic evaluation across multiple behavioral conditions revealed substantial similarity in CeA→SNL and SNL DA neural responses to salient events, suggesting that the net principle effect of CeA→SNL communication is SNL DA neuron activation. An exception to this pattern was the prominent CS responses in SNL DA neurons that were rapidly enhanced by learning, while CeA→SNL CS responses were smaller and slower to develop. Weaker CS responses in CeA→SNL neurons could reflect excitatory responses in a smaller number of cells or a mixed excitatory and inhibitory response in a larger population. Presumably, other excitatory SNL afferents convey additional CS information that is integrated with CeA US signals.

Our findings are consistent with increasing evidence that in addition to encoding reward prediction errors (Schultz, 2016), DA neurons encode other signals that likely serve different functions (Bromberg-Martin et al., 2010; Watabe-Uchida and Uchida, 2018). Single-unit recording studies in non-human primates demonstrate that DA neurons not encoding reward prediction errors cluster dorsolaterally (Matsumoto and Takada, 2013; Kim et al., 2015), including neurons that are activated by rewarding and aversive stimuli which have been proposed to encode motivational salience (Matsumoto and Hikosaka, 2009; Bromberg-Martin et al., 2010). In the mouse, population activity measurements from DA neurons that project to DLS or the posterior extreme of the striatum also reveal unique signals that include prominent encoding of aversive, novel, or physically salient stimuli (Lerner et al., 2015; Menegas et al., 2017, 2018).

Conclusions

Using a multidisciplinary approach to examine amygdala and midbrain DA circuits, we offer insight into an underappreciated connection between two evolutionarily ancient neural systems. Our data suggest that CeA signals modulate emotional responses to salient stimuli via projections to SNL and add to a growing body of evidence that complementary amygdala connections with heterogeneous, topographically organized mesostriatal circuits implement distinct aspects of emotional behavior. Future experiments will further refine the specific connectivity and behavioral roles of subpopulations within CeA→SNL projections and determine how dysfunction of these circuits contributes to deficits in emotion generation and regulation that manifest in neuropsychiatric disease.

STAR★METHODS

Detailed methods are provided in the online version of this paper and include the following:

- KEY RESOURCES TABLE
- LEAD CONTACT AND MATERIALS AVAILABILITY
  - Lead contact
  - Materials availability
- EXPERIMENTAL MODEL AND SUBJECT DETAILS
- METHOD DETAILS
  - Surgical procedures
  - Viral volumes, sources and titers
  - General histological procedures and imaging
  - Axon collateralization analysis
  - Behavioral procedures – gain-of-function
  - Behavioral procedures – photometry
  - Behavioral procedures – loss-of-function
  - Photometry data acquisition
  - *Ex vivo* physiology
  - Single-cell quantitative PCR
- QUANTIFICATION AND STATISTICAL ANALYSIS
  - Statistical methods
  - Analysis and quantification of behavioral data
  - Analysis and quantification of photometry data
- DATA AND CODE AVAILABILITY

SUPPLEMENTAL INFORMATION

Supplemental Information can be found online at https://doi.org/10.1016/j.neuron.2020.03.016.

ACKNOWLEDGMENTS

We thank members of the Malenka and H. Fields laboratories for helpful discussions as well as P. Janak, N. Eshel, and D. Cardozo Pinto for critical feedback on the manuscript. We thank L. Taniguchi for assistance with behavior scoring. This work was funded by an A.P. Giannini Foundation postdoctoral fellowship and NIH K99 Career Development Award (MH116065) to E.E.S.; a Walter V. and Idun Berry postdoctoral fellowship and NARSAD Young Investigator Award to F.G.; an NIH K08 Career Development Award (MH110610) to B.D.H.; an NIH K99 Career Development Award (DA041445) and F32 (DA038913) to K.T.B.; and a grant from the NeuroChoice Big Idea of the Wu Tsai Neurosciences Institute to R.C.M.

AUTHOR CONTRIBUTIONS

E.E.S. and R.C.M. conceptualized the study and wrote the paper with input from all authors. E.E.S. and F.G. performed fiber photometry experiments with support from T.N.L. E.E.S. and B.D.H. performed *ex vivo* physiology experiments. E.E.S., M.D.T., and Z.C.N. performed behavioral optogenetics and pharmacology experiments. K.T.B. analyzed axon collateralization data and provided viral reagents. E.E.S. performed single-cell transcriptomics experiments with support from C.F. L.L. and K.D. provided resources for viral-genetic tracing and fiber photometry experiments, respectively.

DECLARATION OF INTERESTS

The authors declare no competing interests.

Received: March 6, 2019
Revised: February 3, 2020
Accepted: March 18, 2020
Published: April 14, 2020

REFERENCES

Andero, R., Daniel, S., Guo, J.-D., Bruner, R.C., Seth, S., Marvar, P.J., Rainnie, D., and Ressler, K.J. (2016). Amygdala-dependent molecular mechanisms of the Tac2 pathway in fear learning. Neuropsychopharmacology *41*, 2714–2722.

Asok, A., Draper, A., Hoffman, A.F., Schulkin, J., Lupica, C.R., and Rosen, J.B. (2018). Optogenetic silencing of a corticotropin-releasing factor pathway from the central amygdala to the bed nucleus of the stria terminalis disrupts sustained fear. Mol. Psychiatry *23*, 914–922.

Bäckman, C.M., Malik, N., Zhang, Y., Shan, L., Grinberg, A., Hoffer, B.J., Westphal, H., and Tomac, A.C. (2006). Characterization of a mouse strain expressing Cre recombinase from the 3′ untranslated region of the dopamine transporter locus. Genesis *44*, 383–390.

Balleine, B.W., and O'Doherty, J.P. (2010). Human and rodent homologies in action control: corticostriatal determinants of goal-directed and habitual action. Neuropsychopharmacology *35*, 48–69.

Beier, K.T., Steinberg, E.E., DeLoach, K.E., Xie, S., Miyamichi, K., Schwarz, L., Gao, X.J., Kremer, E.J., Malenka, R.C., and Luo, L. (2015). Circuit Architecture of VTA Dopamine Neurons Revealed by Systematic Input-Output Mapping. Cell *162* (3), 622–634.

Berridge, K.C., and Robinson, T.E. (1998). What is the role of dopamine in reward: hedonic impact, reward learning, or incentive salience? Brain Res. Brain Res. Rev. *28*, 309–369.

Bromberg-Martin, E.S., Matsumoto, M., and Hikosaka, O. (2010). Dopamine in motivational control: rewarding, aversive, and alerting. Neuron *68*, 815–834.

Cador, M., Robbins, T.W., and Everitt, B.J. (1989). Involvement of the amygdala in stimulus-reward associations: interaction with the ventral striatum. Neuroscience *30*, 77–86.

Calu, D.J., Roesch, M.R., Haney, R.Z., Holland, P.C., and Schoenbaum, G. (2010). Neural correlates of variations in event processing during learning in central nucleus of amygdala. Neuron *68*, 991–1001.

Ciocchi, S., Herry, C., Grenier, F., Wolff, S.B.E., Letzkus, J.J., Vlachos, I., Ehrlich, I., Sprengel, R., Deisseroth, K., Stadler, M.B., et al. (2010). Encoding of conditioned fear in central amygdala inhibitory circuits. Nature *468*, 277–282.

Corbit, L.H., and Balleine, B.W. (2005). Double dissociation of basolateral and central amygdala lesions on the general and outcome-specific forms of pavlovian-instrumental transfer. J. Neurosci. *25*, 962–970.

Cunningham, C.L., Gremel, C.M., and Groblewski, P.A. (2006). Drug-induced conditioned place preference and aversion in mice. Nat. Protoc. *1*, 1662–1670.

Davis, M. (1992). The role of the amygdala in fear and anxiety. Annu. Rev. Neurosci. *15*, 353–375.

Everitt, B.J., Morris, K.A., O'Brien, A., and Robbins, T.W. (1991). The basolateral amygdala-ventral striatal system and conditioned place preference: further evidence of limbic-striatal interactions underlying reward-related processes. Neuroscience *42*, 1–18.

Fadok, J.P., Krabbe, S., Markovic, M., Courtin, J., Xu, C., Massi, L., Botta, P., Bylund, K., Müller, C., Kovacevic, A., et al. (2017). A competitive inhibitory circuit for selection of active and passive fear responses. Nature *542*, 96–100.

Fadok, J.P., Markovic, M., Tovote, P., and Lüthi, A. (2018). New perspectives on central amygdala function. Curr. Opin. Neurobiol. *49*, 141–147.

Fuccillo, M.V., Földy, C., Gökce, Ö., Rothwell, P.E., Sun, G.L., Malenka, R.C., and Südhof, T.C. (2015). Single-cell mRNA profiling reveals cell-type-specific expression of neurexin isoforms. Neuron *87*, 326–340.

Fudge, J.L., and Haber, S.N. (2000). The central nucleus of the amygdala projection to dopamine subpopulations in primates. Neuroscience *97*, 479–494.

Gallagher, M., Graham, P.W., and Holland, P.C. (1990). The amygdala central nucleus and appetitive Pavlovian conditioning: lesions impair one class of conditioned behavior. J. Neurosci. *10*, 1906–1911.

Han, J.-S., McMahan, R.W., Holland, P., and Gallagher, M. (1997). The role of an amygdalo-nigrostriatal pathway in associative learning. J. Neurosci. *17*, 3913–3919.

Holland, P.C., and Gallagher, M. (1993). Amygdala central nucleus lesions disrupt increments, but not decrements, in conditioned stimulus processing. Behav. Neurosci. *107*, 246–253.

Holland, P.C., and Gallagher, M. (1999). Amygdala circuitry in attentional and representational processes. Trends Cogn. Sci. *3*, 65–73.

Holland, P.C., and Kenmuir, C. (2005). Variations in unconditioned stimulus processing in unblocking. J. Exp. Psychol. Anim. Behav. Process. *31*, 155–171.

Janak, P.H., and Tye, K.M. (2015). From circuits to behaviour in the amygdala. Nature *517*, 284–292.

Keiflin, R., Pribut, H.J., Shah, N.B., and Janak, P.H. (2019). Ventral tegmental dopamine neurons participate in reward identity predictions. Curr. Biol. *29*, 93–103.e3.

Kelley, A.E., and Delfs, J.M. (1991). Dopamine and conditioned reinforcement. I. Differential effects of amphetamine microinjections into striatal subregions. Psychopharmacology (Berl.) *103*, 187–196.

Kim, H.F., Ghazizadeh, A., and Hikosaka, O. (2015). Dopamine neurons encoding long-term memory of object value for habitual behavior. Cell *163*, 1165–1175.

Kim, J., Zhang, X., Muralidhar, S., LeBlanc, S.A., and Tonegawa, S. (2017). Basolateral to central amygdala neural circuits for appetitive behaviors. Neuron *93*, 1464–1479.e5.

Lammel, S., Steinberg, E.E., Földy, C., Wall, N.R., Beier, K., Luo, L., and Malenka, R.C. (2015). Diversity of transgenic mouse models for selective targeting of midbrain dopamine neurons. Neuron *85*, 429–438.

Lee, H.J., Groshek, F., Petrovich, G.D., Cantalini, J.P., Gallagher, M., and Holland, P.C. (2005). Role of amygdalo-nigral circuitry in conditioning of a visual stimulus paired with food. J. Neurosci. *25*, 3881–3888.

Lee, H.J., Youn, J.M., O, M.J., Gallagher, M., and Holland, P.C. (2006). Role of substantia nigra-amygdala connections in surprise-induced enhancement of attention. J. Neurosci. *26*, 6077–6081.

Lerner, T.N., Shilyansky, C., Davidson, T.J., Evans, K.E., Beier, K.T., Zalocusky, K.A., Crow, A.K., Malenka, R.C., Luo, L., Tomer, R., and Deisseroth, K. (2015). Intact-brain analyses reveal distinct information carried by SNc dopamine subcircuits. Cell *162*, 635–647.

Li, B. (2019). Central amygdala cells for learning and expressing aversive emotional memories. Curr. Opin. Behav. Sci. *26*, 40–45.

Li, H., Penzo, M.A., Taniguchi, H., Kopec, C.D., Huang, Z.J., and Li, B. (2013). Experience-dependent modification of a central amygdala fear circuit. Nat. Neurosci. *16*, 332–339.

Lingawi, N.W., and Balleine, B.W. (2012). Amygdala central nucleus interacts with dorsolateral striatum to regulate the acquisition of habits. J. Neurosci. *32*, 1073–1081.

Madisen, L., Zwingman, T.A., Sunkin, S.M., Oh, S.W., Zariwala, H.A., Gu, H., Ng, L.L., Palmiter, R.D., Hawrylycz, M.J., Jones, A.R., et al. (2010). A robust and high-throughput Cre reporting and characterization system for the whole mouse brain. Nat. Neurosci. *13*, 133–140.

Matsumoto, M., and Hikosaka, O. (2009). Two types of dopamine neuron distinctly convey positive and negative motivational signals. Nature *459*, 837–841.

Matsumoto, M., and Takada, M. (2013). Distinct representations of cognitive and motivational signals in midbrain dopamine neurons. Neuron *79*, 1011–1024.

Menegas, W., Babayan, B.M., Uchida, N., and Watabe-Uchida, M. (2017). Opposite initialization to novel cues in dopamine signaling in ventral and posterior striatum in mice. eLife *6*, e21886.

Menegas, W., Akiti, K., Amo, R., Uchida, N., and Watabe-Uchida, M. (2018). Dopamine neurons projecting to the posterior striatum reinforce avoidance of threatening stimuli. Nat. Neurosci. *21*, 1421–1430.

Miyamichi, K., Shlomai-Fuchs, Y., Shu, M., Weissbourd, B.C., Luo, L., and Mizrahi, A. (2013). Dissecting local circuits: parvalbumin interneurons underlie broad feedback control of olfactory bulb output. Neuron *80*, 1232–1245.

Murray, J.E., Belin-Rauscent, A., Simon, M., Giuliano, C., Benoit-Marand, M., Everitt, B.J., and Belin, D. (2015). Basolateral and central amygdala differentially recruit and maintain dorsolateral striatum-dependent cocaine-seeking habits. Nat. Commun. *6*, 10088.

O'Connor, E.C., Stephens, D.N., and Crombag, H.S. (2010). Modeling appetitive Pavlovian-instrumental interactions in mice. Curr. Protoc. Neurosci. *Chapter 8*, Unit 8.25.

O'Doherty, J.P., Cockburn, J., and Pauli, W.M. (2017). Learning, reward, and decision making. Annu. Rev. Psychol. *68*, 73–100.

Phelps, E.A., and LeDoux, J.E. (2005). Contributions of the amygdala to emotion processing: from animal models to human behavior. Neuron *48*, 175–187.

Robinson, M.J.F., Warlow, S.M., and Berridge, K.C. (2014). Optogenetic excitation of central amygdala amplifies and narrows incentive motivation to pursue one reward above another. J. Neurosci. *34*, 16567–16580.

Robledo, P., Robbins, T.W., and Everitt, B.J. (1996). Effects of excitotoxic lesions of the central amygdaloid nucleus on the potentiation of reward-related stimuli by intra-accumbens amphetamine. Behav. Neurosci. *110*, 981–990.

Russell, J.A. (2003). Core affect and the psychological construction of emotion. Psychol. Rev. *110*, 145–172.

Saunders, B.T., Richard, J.M., Margolis, E.B., and Janak, P.H. (2018). Dopamine neurons create Pavlovian conditioned stimuli with circuit-defined motivational properties. Nat. Neurosci. *21*, 1072–1083.

Sawamoto, K., Nakao, N., Kobayashi, K., Matsushita, N., Takahashi, H., Kakishita, K., Yamamoto, A., Yoshizaki, T., Terashima, T., Murakami, F., et al. (2001). Visualization, direct isolation, and transplantation of midbrain dopaminergic neurons. Proc. Natl. Acad. Sci. USA *98*, 6423–6428.

Schultz, W. (2016). Dopamine reward prediction error coding. Dialogues Clin. Neurosci. *18*, 23–32.

Schwarz, L.A., Miyamichi, K., Gao, X.J., Beier, K.T., Weissbourd, B., DeLoach, K.E., Ren, J., Ibanes, S., Malenka, R.C., Kremer, E.J., and Luo, L. (2015). Viral-genetic tracing of the input-output organization of a central noradrenaline circuit. Nature *524*, 88–92.

Shabel, S.J., and Janak, P.H. (2009). Substantial similarity in amygdala neuronal activity during conditioned appetitive and aversive emotional arousal. Proc. Natl. Acad. Sci. USA *106*, 15031–15036.

Sheppes, G., Suri, G., and Gross, J.J. (2015). Emotion regulation and psychopathology. Annu. Rev. Clin. Psychol. *11*, 379–405.

Steinberg, E.E., and Janak, P.H. (2013). Establishing causality for dopamine in neural function and behavior with optogenetics. Brain Res. *1511*, 46–64.

Suarez, M.A. (2012). Sensory processing in children with autism spectrum disorders and impact on functioning. Pediatr. Clin. North Am. *59*, 203–214, xii–xiii.

Taniguchi, H., He, M., Wu, P., Kim, S., Paik, R., Sugino, K., Kvitsiani, D., Fu, Y., Lu, J., Lin, Y., et al. (2011). A resource of Cre driver lines for genetic targeting of GABAergic neurons in cerebral cortex. Neuron *71*, 995–1013.

Taylor, J.R., and Robbins, T.W. (1984). Enhanced behavioural control by conditioned reinforcers following microinjections of d-amphetamine into the nucleus accumbens. Psychopharmacology (Berl.) *84*, 405–412.

Taylor, J.R., and Robbins, T.W. (1986). 6-Hydroxydopamine lesions of the nucleus accumbens, but not of the caudate nucleus, attenuate enhanced responding with reward-related stimuli produced by intra-accumbens d-amphetamine. Psychopharmacology (Berl.) *90*, 390–397.

Tovote, P., Esposito, M.S., Botta, P., Chaudun, F., Fadok, J.P., Markovic, M., Wolff, S.B.E., Ramakrishnan, C., Fenno, L., Deisseroth, K., et al. (2016). Midbrain circuits for defensive behaviour. Nature *534*, 206–212.

Tritsch, N.X., Ding, J.B., and Sabatini, B.L. (2012). Dopaminergic neurons inhibit striatal output through non-canonical release of GABA. Nature *490*, 262–266.

Vankova, M., Arluison, M., Leviel, V., and Tramu, G. (1992). Afferent connections of the rat substantia nigra pars lateralis with special reference to peptide-containing neurons of the amygdalo-nigral pathway. J. Chem. Neuroanat. *5*, 39–50.

Vong, L., Ye, C., Yang, Z., Choi, B., Chua, S., Jr., and Lowell, B.B. (2011). Leptin action on GABAergic neurons prevents obesity and reduces inhibitory tone to POMC neurons. Neuron *71*, 142–154.

Watabe-Uchida, M., and Uchida, N. (2018). Multiple dopamine systems: weal and woe of dopamine. Cold Spring Harb. Symp. Quant. Biol. *83*, 83–95.

Weiskrantz, L. (1956). Behavioral changes associated with ablation of the amygdaloid complex in monkeys. J. Comp. Physiol. Psychol. *49*, 381–391.

Wickersham, I.R., Lyon, D.C., Barnard, R.J.O., Mori, T., Finke, S., Conzelmann, K.-K., Young, J.A.T., and Callaway, E.M. (2007). Monosynaptic restriction of transsynaptic tracing from single, genetically targeted neurons. Neuron *53*, 639–647.

Yu, K., Garcia da Silva, P., Albeanu, D.F., and Li, B. (2016). Central amygdala somatostatin neurons gate passive and active defensive behaviors. J. Neurosci. *36*, 6488–6496.

Yu, K., Ahrens, S., Zhang, X., Schiff, H., Ramakrishnan, C., Fenno, L., Deisseroth, K., Zhao, F., Luo, M.-H., Gong, L., et al. (2017). The central amygdala controls learning in the lateral amygdala. Nat. Neurosci. *20*, 1680–1685.

STAR★METHODS

KEY RESOURCES TABLE

REAGENT or RESOURCE	SOURCE	IDENTIFIER
Antibodies		
Tyrosine Hydroxylase (TH), rabbit	Millipore	RRID: AB_390204
Tyrosine Hydroxylase (TH), sheep	Millipore	RRID: AB_90755
GFP, sheep	Novus Biologicals	RRID: AB_1048872
GFP, chicken	Aves labs	RRID: AB_10000240
mCherry, rat	Invitrogen	M11217
Bacterial and Virus Strains		
CAV2-Cre	IGMM Vector Core	Lot# 01/28/15
AAV5-Ef1a-DIO-eYFP	UNC Vector Core	Lot# 5083
AAV5-hsyn-mCherry	UNC Vector Core	Lot# 5034D
AAV5-hsyn-ChR2(H134R)-eYFP	UNC Vector Core	Lot# 5580, 4319G/H/I
AAV5-hsyn-NpHR3.0-eYFP	UNC Vector Core	Lot# 4321C
AAV5-hsyn-eYFP	UNC Vector Core	Lot# 4836B, 4836D
AAVDJ-Ef1a-DIO-ChR2(H134R)-eYFP	Stanford Vector Core	Lot# 4176
AAVDJ-Ef1a-DIO-GCaMP6f	Stanford Vector Core	Lot# 1858, 2364
AAV5-Ef1a-FLEX-tdTomato	UNC Vector Core	Lot# 4599C
AAV8-CAG-FLEX-RabiesG	UNC Vector Core	Lot# 6536B
AAV2-FLEX-TC^{66T}	Stanford Vector Core	N/A
RVΔG-GFP+EnvA	Custom prep, L. Luo lab	N/A
AAV8-Ef1a-DIO-GCaMP6m	Stanford Vector Core	Lot# 2149
AAVDJ-Ef1a-DIO-ChR2(H134R)-mCherry	Stanford Vector Core	Lot# 4215
Chemicals, Peptides, and Recombinant Proteins		
Tetrodotoxin citrate	Tocris	1069-1mg
4-aminopyridine	Sigma	A78403-25 g
Picrotoxin	Sigma	P1675-5G
Muscimol	Sigma	M1523-5MG
Baclofen	Sigma	B5399-500MG
Critical Commercial Assays		
48x48 Dynamic Array IFC for Gene Expression	Fluidigm	BMK-M-48.48
Experimental Models: Organisms/Strains		
Wild-type C57BL/6J	The Jackson Laboratory	RRID: IMSR_JAX:000664
DAT^{IREScre} (B6.SJL-*Slc6a3*$^{tm1.1(cre)Bkmn}$/J)	The Jackson Laboratory	RRID: IMSR_JAX:006660
Vgat^{IREScre} (B6J.129S6(FVB)-*Slc32a1*$^{tm2(cre)Lowl}$/MwarJ)	The Jackson Laboratory	RRID: IMSR_JAX:028862
Ai14 (B6.Cg-*Gt(ROSA)26Sor*$^{tm14(CAG-tdTomato)Hze}$/J)	The Jackson Laboratory	RRID: IMSR_JAX:007914
SOM^{IREScre} (SOM$^{tm2.1(cre)Zjh}$/J)	The Jackson Laboratory	RRID: IMSR_JAX:013044
Th^{GFP} (Tg(Th-EGFP)6-7Okn)	Gift of P. Janak	MGI: 5604271

LEAD CONTACT AND MATERIALS AVAILABILITY

Lead contact

Further information and requests for resources and reagents should be directed to and will be fulfilled by the lead contact, Dr. Robert Malenka (malenka@stanford.edu).

Materials availability

This study did not generate new unique reagents.

EXPERIMENTAL MODEL AND SUBJECT DETAILS

All experimental procedures were approved by the Stanford University Institutional Animal Care and Use Committee (IACUC). All mice used in this study were on a C57BL/6J background, typically group-housed with littermates of the same sex, and given access to food and water *ad libitum* except where noted below. Adult male wild-type mice > 8 weeks of age were used for behavioral experiments except where sex differences were directly examined (Figure S2C). For studies involving *Sst*:Cre mice, males and females were used. Behavioral testing was performed during the light cycle (lights on 07:00, off at 19:00). For anatomy and physiology experiments, male and female mice > 8 weeks of age were used. The following mouse lines were used in this study: wild-type C57BL/6J (strain 000664), DAT:IRES-Cre (strain 006660), Vgat:IRES-Cre (strain 028862), Ai14 Cre-reporter (strain 007914), *Sst*:IRES-Cre (strain 013044), all originally sourced from The Jackson Laboratory. Additionally, TH:GFP mice (gift of P. Janak) were used in some experiments to facilitate identification of dopamine neurons. Heterozygous DAT:Cre, Vgat:Cre or *Sst*:Cre mice, or double heterozygous Vgat:Cre x Th:GFP mice were used for all experiments. These lines were maintained by backcrossing to C57BL/6J wild-types. Homozygous Ai14 Cre-reporter mice were used for retrograde labeling experiments including qPCR.

METHOD DETAILS

Surgical procedures

Injection and implant surgeries were performed under ketamine-medetomidine anesthesia using a stereotaxic instrument (Kopf Instruments). A small incision was made in the scalp and burr holes were drilled in the skull at the appropriate stereotaxic coordinates (AP and ML relative to bregma; DV relative to skull surface at target coordinate): −1.2 AP, ± 2.6-2.9 ML, −4.3 DV for CeA; −2.8 AP, ± 1.9 ML, −3.9 DV for SNL, +0.14 AP, ± 0.9 ML, −4.8 DV for BNST; −4.2 AP, ± 0.5 ML, −2.9 DV for PAG. Bregma-lamda distance was measured and a correction factor [(B-L distance)/4.2 x AP coordinate] was used if the measured distance differed from 4.2mm. Viruses were infused using a glass micropipette connected to a syringe pump (Harvard Apparatus) at a rate of 125nl/min via tubing back-filled with mineral oil. The injector tip was lowered an additional 0.1mm below the planned injection site and then raised to the final coordinate prior to infusion to facilitate virus diffusion at the site of injection, instead of along the needle track. The injection pipette was slowly withdrawn 5-10 min after the end of the infusion. For optogenetic and photometry experiments, a fiber optic was also implanted over the CeA or SNL. For optogenetic experiments, the optical fiber was targeted ∼300 μM above CeA axon terminals. For intra-CeA pharmacology experiments, 26 ga guide cannula (Plastics One) were implanted at a 15° angle (−1.2 AP, ± 3.975 ML, −2.85 DV); a drug infuser was acutely inserted prior to behavioral experiments that protruded a further 1.5 mm for a final DV coordinate of −4.35 mm. For photometry experiments the optical fiber was targeted ∼100 μM above the virus injection site. Unilateral optogenetic manipulations were targeted to the left hemisphere. Intracranial implants were affixed to the skull using small screws (Antrin Miniature Specialties) and epoxy (Geristore, DenMat). For optogenetic excitation experiments, optical implants and cables were made in-house using 200 μm core, 0.39 NA fiber (FT200EMT, Thorlabs). For optogenetic inhibition experiments, implants (250 μm core, 0.66 NA) were purchased from Prizmatix. For photometry experiments, low-autofluorescence optical implants and cables (400 μm core, 0.48 NA) were purchased from Doric Lenses.

Viral volumes, sources and titers

For anterograde tracing experiments, 0.2 μl of AAV5-hsyn-eYFP (UNC Vector Core, 3.5×10^{12} particles/ml) was injected into the CeA in wild-type mice. > 8 weeks later, animals were sacrificed for analysis.

For axon collateralization analysis, 0.2 μl of CAV2-Cre (IGMM Vector Core, France, 4.2×10^{12} particles/ml) was injected in the SNL and 0.2-0.4 μl of AAV5-Ef1a-DIO-eYFP (UNC Vector Core, 4×10^{12} particles/ml) was injected into the CeA in the left hemisphere. In the right hemisphere, 0.2 μl of AAV5-hsyn-mCherry (UNC Vector Core, 3.4×10^{12} particles/ml) was injected into the CeA in wild-type mice. 14 weeks later, animals were sacrificed for analysis.

For retrograde labeling experiments, including qPCR studies, 0.2 μl of CAV2-Cre (IGMM Vector Core, France, 4.2×10^{12} particles/ml) was injected in the SNL, BNST or PAG of Ai14 Cre-reporter mice. > 5 days later, animals were sacrificed for analysis or used for mRNA measurements.

For optogenetic activation experiments, 0.2ul of AAV5-hsyn-ChR2(H134R)-eYFP (UNC Vector Core, 4.6×10^{10} to 5.5×10^{12} particles/ml) or 0.2ul of AAV5-hsyn-eYFP (UNC Vector Core, 3.5×10^{12} particles/ml) was unilaterally or bilaterally injected into the CeA and optical fibers were implanted above axon terminals in SNL in wild-type mice. For experiments in *Sst*:Cre mice, 0.2ul of AAVDJ-Ef1a-DIO-ChR2(H134R)-eYFP (Stanford Vector Core, 6.4×10^{12} particles/ml) was injected into the CeA and optical fibers were bilaterally implanted above the SNL.

For photometry experiments targeting CeA-SNL neurons, 0.2 μl of CAV2-Cre (IGMM Vector Core, France, 4.2×10^{12} particles/ml) was unilaterally injected in the SNL and 0.5-0.7 μl of AAVDJ-Ef1a-DIO-GCaMP6f (Stanford Vector Core, 1×10^{14} particles/ml) was unilaterally injected into the CeA. An optical fiber was implanted dorsal to cell bodies in CeA in WT mice.

For optogenetic inhibition experiments, 0.2ul of AAV5-hsyn-NpHR3.0-eYFP (UNC Vector Core, 7.7×10^{12} particles/ml) or 0.2ul of AAV5-hsyn-eYFP (UNC Vector Core, 6.6×10^{12} particles/ml) was bilaterally injected into the CeA and optical fibers were implanted above axon terminals in SNL in wild-type mice.

For cell type-specific monosynaptic rabies tracing, 0.125 μl of a 1:1 mix of AAV8-CAG-FLEX-RabiesG (UNC Vector Core, 1.8×10^{12} particles/ml) and AAV2-CAG-FLEX-TC^{66T} (Stanford Vector Core, 1.0×10^{12} particles/ml) was injected into the SNL in DAT:Cre or Vgat:Cre mice. Two weeks later, 0.375 μl of RVΔG-GFP+EnvA (custom prep, L. Luo lab, 1.3×10^{9} colony forming units/ml) was injected at the same site. 5 days later, animals were sacrificed for analysis.

For *ex vivo* electrophysiology experiments mapping CeA→SNL connections, 0.2 μl of AAV5-hsyn-ChR2(H134R)-eYFP (UNC Vector Core, 4.8×10^{12} particles/ml) was injected into the CeA and 1.0 μl of AAV5-FLEX-tdTomato (UNC Vector Core, 4.8×10^{12} particles/ml) was injected into the SNL in DAT:Cre, Vgat:Cre or Vgat:Cre x Th:GFP mice. A DV coordinate of 4.4 was used for SNL targeting for this experiment to facilitate Cre-dependent viral labeling throughout the SNL and surrounding areas. For experiments mapping local connections within the substantia nigra, 0.2 ul of AAVDJ-Ef1a-DIO-ChR2(H134R)-mCherry (Stanford Vector Core, 5.6×10^{12} particles/ml) was injected into the SNL of Vgat:Cre x Th:GFP mice.

For photometry experiments targeting SNL DA neurons either 0.5 μl of AAVDJ-Ef1a-DIO-GCaMP6f (Stanford Vector Core, 1×10^{14} particles/ml) or 0.2 μl of AAV8-Ef1a-DIO-GCaMP6m (Stanford Vector Core, 3×10^{13} particles/ml) was unilaterally injected into the SNL. An optical fiber was implanted dorsal to cell bodies in SNL in DAT:Cre mice.

General histological procedures and imaging

Mice were deeply anesthetized with sodium pentobarbital and transcardially perfused with 4% paraformaldehyde. Brains were removed, post-fixed for 24 hours and sectioned at room temperature on a vibratome with the exception of brains for axon collateralization and rabies tracing experiments, which were cryoprotected in 30% sucrose for 24-48 hours and sectioned on a cryostat. Free-floating 60 μm sections were processed for TH and YFP immunohistochemistry. Sections were incubated in a blocking solution (BS) containing bovine serum albumin and Triton X-100 (each 0.2%) in PBS for 20 min. Normal donkey serum (NDS) (10%) was added to BS for a further 30 min incubation. Sections were then incubated overnight with primary antibodies, followed by a 3 hr incubation with secondary antibodies (all at room temperature). Sections were washed and mounted on microscope slides, and coverslipped with Fluoromount-G mounting medium (Southern Biotech). Concentrations and sources for antibodies were as follows: rabbit anti-TH 1:1500 (Millipore, AB152) or sheep anti-TH 1:4000 (Millipore AB 1542), sheep anti-GFP 1:3000 (Novus Biologicals, NB110-75114) or chicken anti-GFP 1:1000-2000 (Aves labs, GFP-1020), rat anti-mCherry 1:1000-2000 (Invitrogen, M11217), donkey anti-rabbit, sheep, chicken or rat secondary antibodies 1:200 (Invitrogen or Jackson ImmunoResearch). Sections were visualized on a Nikon A1 confocal microscope. When quantitative or qualitative comparisons were made between images, all image acquisition and post-processing settings were held constant.

For optogenetic experiments, although optical fiber placement varied slightly between animals, no subjects were excluded due to targeting. Two subjects were excluded due to complete virus injection failure (no detectable fluorophore expression in CeA). For photometry experiments, 7 CeA-SNL and 3 SNL DA mice were excluded due to poor photometry signal. Histological analysis confirmed this was due to weak virus expression and/or optical fibers not aligned with GCaMP6 expressing cells.

Axon collateralization analysis

After antibody staining for GFP and mCherry, sections were mounted and whole slides were imaged with a 5x objective using a Leica Ariol slide scanner with the SL200 slide loader. For analysis, the method of Beier et al., 2015 was followed. Briefly, the background was first subtracted and the mean of local background after subtraction was multiplied by a constant value of 4. This was defined as the threshold, with pixels above this gray-scale value interpreted as positive signal from amygdala axons. The threshold value was kept constant for all sections analyzed within a brain. Axon density, defined as the percentage of total ROI containing pixels above threshold, was quantified using ImageJ. 3 sections were analyzed per ROI and these values were averaged to calculate a single value per ROI per mouse; values from 5 mice were averaged to generate the graph in Figure 1D. ROI boundaries were manually defined based on DAPI staining and the Franklin and Paxinos mouse brain atlas, 3rd edition.

Behavioral procedures – gain-of-function

Stimulation parameters

Prior to behavioral sessions, mice were habituated to handling (> 3 days) and were gently attached to patch cables made in-house with optical fiber (0.39 NA, 200 μm diameter, Thorlabs) via a ceramic split sleeve (Precision Fiber Products). The patch cables were also connected to unilateral or bilateral rotary joints (Doric Lenses), which permitted free rotation while transmitting blue light from an upstream 473 nm laser (Laserglow). Peak light output during photostimulation was estimated to be ~2.75 mW at the tip of the implanted fiber (~22 mW/mm^2). This value was derived by measuring the average light power for the pulsed light parameters used during experiments (typically 20 Hz, 5 ms pulse duration), and then correcting for the duty cycle to arrive at the peak power (in this case by dividing by 0.1). The power density estimate was based on the light transmission calculator at http://www.stanford.edu/group/dlab/optogenetics/calc.

Intracranial self-stimulation

Experimental sessions were conducted in operant conditioning chambers (24 cm W x 20 cm D x 18 cm H, Med Associates Inc.) contained within sound-attenuating cubicles. The left side of the chamber was fitted with 5 nosepoke ports, each with an LED light at the rear. Optical stimulation was controlled by a computer running Med PC IV software (Med Associates Inc.), which also recorded responses at nosepoke ports. Prior to the first behavioral session, mice were familiarized with cereal treats (Froot Loops, Kellogg) in

their home cage. On the first training day, all nosepokes were baited with crushed cereal treats to facilitate initial investigation, with the exception of the experiment reported in Figures S2M and S2N. For this study, appetitive stimuli would have impacted latency measurements on the first training day and were not used. Session length was 60 min (except for Figures S2M and S2N where it was 30 min to mirror the timing of CPP procedures), during which time mice were free to respond at any nosepoke port. 4 ports were designated "active" ports, and a response at these ports produced 2 s of optical stimulation (1, 5, 10 or 20 Hz, 5ms pulse width in all cases); the LED at the back of the corresponding port was concurrently illuminated to provide a visual cue signaling the presence of optical stimulation. Responses made within the 2 s stimulation period were recorded but had no consequence. Responses at a 5th "inactive" nosepoke port were recorded but did not result in either optical stimulation or cue light presentation. In some experiments, only 2 choices (0 Hz or 20Hz) were available; the other three nosepoke ports were closed off. Testing occurred once per day for 5 days and port/frequency assignment was counterbalanced. For the 20 min ICSS extinction test in Figures S2N–S2O, nosepokes did not result in either laser activation or LED cue light presentation.

Intra-CeA pharmacology

After stable ICSS behavior was established, mice were habituated to the infusion procedure with a sham infusion, where a 33 ga infusion cannula (Plastics One) was inserted into the implanted guide cannula and the mouse was restrained but no liquid was infused. For this session, the infuser was cut so as not to protrude past the end of the guide cannula. Subsequently, 0.25 μl saline or muscimol/baclofen (0.1 mM/1.0 mM) was infused bilaterally into the CeA in test sessions spaced 24 hours apart; the saline infusion was performed first. Infusions were made at a rate of 0.25 μl/min with a syringe pump (Harvard Apparatus) and the infusion cannula was left in place for an additional minute to permit drug diffusion. After each infusion, mice were returned to their home cages for 10 min to allow drugs to take effect before behavioral sessions began.

Real-time place preference

For RTPP tests, a 70 cm x 23 cm arena divided into 2 compartments by a partial barrier was used. The left and right compartments were identical and the side initially paired with stimulation was randomly assigned each day. Optical stimulation was controlled by a computer running Biobserve software, which tracked animal position and triggered light delivery via a Master-8 pulse stimulator (A.M.P.I). Initially, the mouse was placed in the non-stimulated compartment with the rest of the arena closed off. After 2 min, the barrier was removed and the mouse was free to explore the entire arena for the remainder of the test. Every time the mouse crossed to the stimulation-paired side of the chamber, pulsed light was delivered at the specified frequency until the mouse crossed back into the other side. For reversal experiments the side paired with stimulation was switched; there was no interruption between the initial and the reversal phases of the experiment. Total test length was 30-40 min (either 15 or 20 min initial/reversal phases). Various stimulation frequencies were tested in the same mice across multiple days; distinct contextual cues (visual and tactile) were used each day to minimize generalization between tests.

Conditioned place preference

For CPP tests a standard unbiased procedure was used (Cunningham et al., 2006). A 70 cm x 23 cm arena was divided into 3 compartments (left, center, right); the left and right compartments had distinct tactile and visual cues which were kept consistent for the entire experiment. On Day 1, a baseline preference test was conducted. The mouse was initially placed in the neutral center compartment with barriers preventing access to other areas. After 2 min, the barriers were removed and the mouse was free to explore the entire arena for 15 min. Mice were connected to optical cables for this test but the laser was turned off.

For optogenetic Pavlovian conditioning (1 or 3 days, as specified), two conditioning sessions were conducted per day, separated by at least 4 hours. In the first session, the mouse was confined to either the left or right compartment and laser was turned on for 30 min. In the second session, the mouse was attached to the optical cables and confined in the other compartment for 30 min but the laser was switched off. The temporal order of testing (stimulation first or second) and stimulation-paired side (left or right) were counterbalanced; ChR2 and eYFP groups were tested in interleaved sessions. For the post-conditioning test (Test 1), the same procedure for the baseline test was followed. Immediately after this 15 min test, an RTPP test (Test 2) was conducted where entries into the previously light-paired side now triggered stimulation as described above. Biobserve software was used to track animal position for baseline and post-conditioning tests and trigger the laser during RTPP.

For the hybrid instrumental-CPP procedure (Figure 2J), the same protocol was followed except that a single 30 min conditioning session was administered each day for 3 days. In this session the mouse was able to freely explore the entire arena and stimulation was turned on whenever the mouse crossed into the stimulation-pared compartment. The experiments shown in Figures 2I and 2J were run in interleaved groups to facilitate direct comparison.

Cocaine CPP (Figure S2K) was performed in the same mice used for the 1-day optogenetic CPP procedure (Figure S2I). For conditioning, either a single injection of cocaine (20mg/kg) or saline vehicle was administered just before placing the animal in one of the distinct compartments. These tests were conducted 24 hours apart to allow for drug wash-out. Baseline and post-conditioning tests were conducted as described above; mice were not attached to optical cables at any point.

Conditioned reinforcement

Mice used for conditioned reinforcement testing had unilateral virus injections and fiber placements to avoid locomotor effects associated with bilateral stimulation. Experimental sessions were conducted in operant conditioning chambers (24 cm W x 20 cm D x 18 cm H, Med Associates Inc.) contained within sound-attenuating cubicles. The right side of the chamber was fitted with two retractable levers flanking a central speaker; an LED cue light was positioned above each lever. Levers remained retracted during the Pavlovian training phase.

To acclimate the mice to the chambers, conditioning cue and tethering with optogenetic cables, during an initial habituation session the cue was presented alone (25 trials, VI 75 s schedule) with no other consequences. Subsequently, mice were given 10 days of Pavlovian training during which the 10 s tone-light cue (75 dB white noise + either left or right cue light, counterbalanced) was presented for 25 trials/day on a VI 75 s schedule. During the last 5 s of the cue, 20 Hz optical stimulation was delivered for "Paired" groups; for the unpaired control group, stimulation was delivered with pseudorandom timing during the ITI and never overlapped with the cue. Pavlovian training sessions were ~37 min in length. For all groups, cue and laser presentations were never contingent on the mouse's behavior and the same number of stimuli (cue and laser presentations) were delivered to all subjects. These parameters were chosen based on published protocols that produce robust conditioned reinforcement for natural rewards in mice (O'Connor et al., 2010) and optogenetic conditioned reinforcement in rats (Saunders et al., 2018).

24 hours after the last Pavlovian training session, mice were given a 60 min conditioned reinforcement test. Both levers were inserted into the chamber for the first time and responses on the active lever (left or right, same side as LED cue light) were reinforced with a 3 s tone-light cue presentation. Responses on the inactive lever were recorded but had no consequence. Mice were attached to optical cables as usual for this test but the lasers were switched off. The next day, mice were given a 60 min primary reinforcement test. Both levers were again inserted into the chamber and presses on the active lever were now reinforced with 3 s of 20 Hz optical stimulation; inactive lever presses had no effect. Cue presentation and optical stimulation were controlled by a computer running Med PC IV software (Med Associates Inc.), which also recorded lever presses during conditioned and primary reinforcement tests. Subsequently, mice were tested for RTPP as described above.

Open field

Mice were allowed to explore a square arena (28 cm x 28 cm for bilateral, 40 cm x 40 cm for unilateral) while various stimulation frequencies were applied. Distance traveled was tracked via Biobserve software. For the bilateral locomotion test, the test length was 27 min, divided into 3 min epochs of alternating light off-on-off. For the unilateral locomotion test, the test length was 15 min, divided into 5 min epochs of alternating light off-on-off.

Behavioral procedures – photometry

Appetitive training

Behavioral training began 1-3 weeks after surgery; Photometry recordings were made 2-8 weeks after surgery. Mice were habituated to handling (> 3 days) prior to the start of the study. Appetitive sessions were conducted in operant conditioning chambers (15 cm W x 13 cm D x 18 cm H, Med Associates Inc.) contained within sound-attenuating cubicles with the exception of the lickometer assay. The right side of the chamber was fitted with 2 levers flanking an extra-tall reward port to allow head entry while attached to optical cables. A speaker was mounted on the back wall. Mice were water restricted to ~1ml/day (maintained at > 85% *ad libitum* weight) and pre-trained to retrieve sucrose rewards (10% w/v) from the reward port while attached to optical cables. Subsequently, mice were trained on either appetitive instrumental or Pavlovian tasks. For instrumental learning, mice were initially trained to press a lever for sucrose (0.7 s pump activation time corresponding to ~25 μl per reward) on a fixed-ratio 1 schedule in daily 1 hour sessions. Once this association had been stably acquired and mice were earning > 40 rewards per session (2-6 days), the schedule was increased to VI60. Data shown are from the 3rd-5th VI60 session.

For Pavlovian learning, an auditory tone (white noise or 4500 Hz pure tone, ~75-80 dB, counterbalanced with aversive CS) was presented for 30 s and sucrose (1.4 s pump activation time corresponding to ~50 μl per reward) was delivered 5 s after cue onset. 20 trials were presented per day with a variable ITI of 2.5 min (51 min total session length). During the Pavlovian appetitive extinction test, identical procedures were followed except the sucrose syringe was not loaded and reward was not delivered. Following Pavlovian or instrumental training, variable reward and lickometer tests were conducted in a subset of mice. For variable reward training, small, medium and large sucrose rewards (0.35, 0.7 or 1.4 s pump activation time, corresponding to ~12.5, 25 or 50 μl volume) were delivered on a VI 45 s schedule in interleaved trials. To prevent multiple rewards from accumulating and ensure that reward consumption was accurately tracked, once a reward was delivered, the interval schedule for the next reward did not start until a port entry had been made. 12 rewards of each size were delivered over a ~30 min session (dependent on the subjects' behavior). For the lickometer test, a drop of sucrose (~10 μl) was made available at a lickometer spout (the only object in a 32 cm x 20 cm arena) on a VI 30 s schedule for 50 trials and individual licks were tracked. As with variable reward training, the next sucrose reward was not delivered until the previous reward had been consumed. For all appetitive sessions, the reward port/lickometer spout was confirmed to be dry at the end of the session indicating that all sucrose had been consumed. Following the conclusion of appetitive testing *ad libitum* water access was restored.

Aversive training

Different conditioning chambers were used for aversive training (19 cm W x 19 cm D x 33 cm H, Coulbourn Instruments). During the aversive Pavlovian training session, an auditory tone (white noise unless this had already been used as the appetitive CS, in which case a 4500 Hz pure tone was used, ~75-80 dB) was presented for 30 s for 4 habituation trials. Subsequently, 6 conditioning trials were given where the tone was followed by a mild footshock (0.3 mA, 1 s, onset coinciding with tone offset). The average ISI between tones was 100 s; total session length was ~18 min. 250 μl of white vinegar (Heinz) was placed on a paper towel in the bedding pan to create a distinct acquisition context. The next day, a retrieval/extinction test was conducted in a new context (distinct walls and floor, 250 μl raspberry extract (McCormick)). The aversive CS was presented alone 12 times with an average ISI of 120 s; total session length was ~23 min. Immediately following this session, the floor covering was removed, exposing the original shock bar floor

and the variable shock session was conducted. During this session, small, medium and large shocks (0.5, 1 or 2 s, all 0.3mA, 5 each) were delivered in interleaved trials with a 45 s variable ISI. The following day, in another new context (distinct walls and scent, 250 μl vanilla extract (McCormick)), 6 shocks of constant length and intensity (2 s, 0.3 mA) were delivered with a variable 90 s ISI to examine the neural response to successive presentations of the same US in the absence of predictive cues.

Behavioral procedures – loss-of-function

Optogenetic loss-of-function studies closely followed the photometry behavior procedures with minor exceptions noted below. These studies commenced > 8 weeks after surgery to allow adequate time for viral expression at axon terminals.

Inhibition parameters

Mice were gently attached to optical patch cables (0.63 NA, 500 μm diameter, Prizmatix) via a ceramic split sleeve. The patch cables were connected to a rotary joint (Prizmatix), which permitted free rotation while transmitting green light from an upstream 545 nm fiber-coupled LED (Prizmatix). Light output was estimated to be ~4-6 mW (~25 mW/mm^2) at the tip of the implanted fiber (0.66 NA, 250 μm diameter, Prizmatix). Constant illumination was used for the time periods specified for each behavioral assay.

Appetitive training

Experimental sessions were conducted in operant conditioning chambers (24 cm W x 20 cm D x 18 cm H, Med Associates Inc.) contained within sound-attenuating cubicles. Mice were food restricted to ~2.5g standard chow/day (maintained at > 85% *ad libitum* weight) and sucrose (10% w/v) solution was used as a reward. The entire cohort of mice progressed sequentially through instrumental and Pavlovian training. Two subjects (n = 1 each NpHR/eYFP) were excluded from analysis for the instrumental tests because they failed to acquire the task (< 2 active lever presses per session). For appetitive instrumental tests, light was triggered when the mouse entered the port following reward delivery and remained on until the mouse exited the port. To ensure close alignment of illumination with sucrose consumption, following reward delivery all port entries would trigger light until the mouse sustained a port entry for 3 s, which was the empirically determined time required to consume sucrose in pilot studies. Once this criterion had been satisfied, further port entries would not trigger light until another reward had been delivered. Mice were initially trained to press a lever in four FR1 and one VI30 sessions before the schedule was increased to VI60. Data from all VI60 sessions are shown.

For appetitive Pavlovian training, white noise (~70 dB) was used as the CS for all mice. Light was applied for the entire 30 s duration of the CS, which included the US delivery period. If a 3 s port entry was not made during the CS, port entries following the CS would also trigger light delivery until the criterion was satisfied.

Sucrose consumption test

A drop of sucrose (~10 μl) was made available at a lickometer spout on a VI 3 s schedule and individual licks were tracked during a 20 min test. The first lick after sucrose delivery triggered 1 s illumination. To ensure close alignment between sucrose consumption and inhibition, the next drop was not delivered until the previous reward had been consumed. Mice were tested with light off and on (order counterbalanced) to evaluate within-subject effects.

Real-time place preference and open field testing

Ad libitum food access was restored prior to the onset of RTPP, open field measurements, and aversive training. Open field tests were conducted in a 40 cm x 40 cm arena. Testing was performed as described for optogenetic activation experiments except that continuous illumination was used for the specified time period.

Aversive training

Aversive training was conducted last. The CS consisted of 500ms tone sweeps (2-6 kHz, ~72 dB) pulsed at 1Hz. The US was a 1 s 0.6 mA footshock that coincided with CS offset. To suppress the full extent of CS and US signals observed in photometry studies, light was applied for 40 s beginning at CS onset during habituation, conditioning, and retrieval 1 trials. Light was not turned on for retrieval 2 tests.

Photometry data acquisition

Following the methods used in Lerner et al. (2015) we measured bulk fluorescence from deep brain regions using a single optical fiber for both delivery of excitation light and collection of emitted fluorescence. The fluorescence output of GCaMP6 is modulated by varying the intensity of the excitation light, generating an amplitude-modulated fluorescence signal that is demodulated to recover the original response. Multiple wavelengths (490nm and 405nm, Thorlabs M490F1 and M405F1) were delivered through the same fiber, each modulated at a distinct carrier frequency, to allow for simultaneous multicolor measurements. 490nm excitation was used to measure calcium-dependent fluorescence changes reflecting neural activity; 405nm excitation was used to measure calcium-independent changes and served as an internal control to correct for motion artifacts and bleaching. LEDs were controlled via an RX8 real-time processor (Tucker Davis Technologies) running custom software. 490nm excitation was sinusoidally modulated at 211Hz and passed through a GFP excitation filter (Thorlabs, MF469-35); 405nm excitation was modulated at 330Hz and passed through a 405nm bandpass filter (Thorlabs, FB405-10). Each LED was coupled into a 0.39NA, 200 μm optical fiber, collimated, and then combined with a 425nm long-pass dichroic mirror (Thorlabs, DMLP425). The excitation light was passed through a 495nm long-pass dichroic mirror (Semrock, FF495-Di03) and coupled into low-autofluorescence 400μm 0.48NA optical cables with opaque covering (Doric lenses) using a fixed-focus 0.51NA coupler/collimator

(Thorlabs, F240FC-A). The GCaMP6 emission signal was collected through the patch cord and collimator, transmitted through the 495nm dichroic, passed through a GFP emission filter (Thorlabs, MF535-39) and focused onto a femtowatt photoreceiver (Newport, Model 2151) using a lens (Edmund Optics, Cat. No. 62-561). The photoreceiver signal was sampled at 6.1 kHz, and each of the two modulated signals generated by the LEDs was independently recovered using standard synchronous demodulation techniques implemented on the RX8 processor. The resulting fluorescence magnitude signals were then decimated to 382 Hz for recording to disk and further filtered using a 2Hz low-pass filter before analysis. Behavioral events (reward port entries detected by infrared beam break, lever presses, cue and shock onset) triggered TTL pulses which were fed into the real-time processor for alignment with photometry signals. Files were then exported for analysis into MATLAB (Mathworks).

Ex vivo physiology

4-6 weeks after injections, mice were deeply anesthetized with sodium pentobarbital and transcardially perfused with ice-cold sucrose artificial cerebrospinal fluid (ACSF) containing (in mM): 50 sucrose, 125 NaCl, 25 $NaHCO_3$, 2.5 KCl, 1.25 NaH_2PO_4, 0.1 $CaCl_2$, 4.9 $MgCl_2$, and 2.5 glucose (oxygenated with 95% O_2/5% CO_2). Coronal midbrain slices (250 μm) containing the SNL were cut in the same solution at 4°C on a vibratome (Leica) and were allowed to recover for 60 min at 33°C, and then for a further 30 min at room temperature. Slices containing the CeA were fixed in 4% PFA and saved for verification of the ChR2 injection site if applicable. For recording, slices were transferred to a recording chamber and perfused continuously at 2-4 ml/min with oxygenated ACSF (in mM): 125 NaCl, 25 $NaHCO_3$, 2.5 KCl, 1.25 NaH_2PO_4, 11 glucose, 1.3 $MgCl_2$ and 2.5 $CaCl_2$. Cells were visualized with a 40x water-immersion objective on an upright fluorescent microscope (BX51WI; Olympus) equipped with infrared-differential interference contrast video microscopy and epifluorescence (Olympus). All recorded cells were verified as tdTomato+ or GFP+ at the time of recording; this was confirmed with posthoc histology. To isolate monosynaptic connections, TTX (0.5 μM) and 4-AP (100 μM) were added to the external solution as per standard protocols (e.g., (Tritsch et al., 2012)). In some cases picrotoxin (100 μM) was also added to block inhibitory currents mediated by GABA-A receptors. Patch pipettes (2.5-4.5 MΩ) were pulled from borosilicate glass (G150TF-4; Warner Instruments) and filled with internal solution containing (in mM): 120 $CsMeSO_3$ 20 HEPES, 0.4 EGTA, 2.8 NaCl, 5 TEA-Cl, 5 QX314-Br, 4 Mg-ATP, 0.4 Na-GTP, 8 Na_2-phosphocreatine, 0.2% w/v biocytin, pH 7.3 (290-295 mOsm).

Whole-cell patch clamp recordings were made at 30-32°C using a MultiClamp700B amplifier and Axograph software; series resistance was typically 15-25 mΩ. To record IPSCs, neurons were voltage-clamped at 0mV. ChR2-expressing axons were stimulated using blue light pulses (5ms pulse width, 50ms ISI, 2 pulses) which were generated using an LED (470nm, Thorlabs) and delivered to the slice via a 40x objective focused on the recorded neuron. Light intensity was kept constant for quantitative comparison of DAT:Cre and Vgat:Cre recordings. Pairs of light pulses were delivered once every 10 s. Response sizes were calculated by baseline-subtracting and averaging 5-15 traces together, then calculating the peak amplitude in a 20ms window after the light pulse. Neurons for which the peak value was < 10pA were considered to be not connected. To verify the neurochemical identity and location of each cell, slices were transferred to 4% PFA after recording and processed for TH immunohistochemistry. The immunohistochemical procedures described above were followed except that primary and secondary antibody incubation times were increased to 48 hours each at 4°C and Streptavidin conjugated to Dylight405 (Invitrogen) was included with the secondary antibodies to detect biocytin.

Single-cell quantitative PCR

For mRNA isolation, acute brain slices were prepared following standard protocols and allowed to recover for 1 hour at room temperature. Cytoplasm from tdTomato+ (i.e., retrogradely labeled) individual CeA neurons was manually aspirated into 2x CellsDirect buffer (Invitrogen) using glass patch pipettes. Samples were snap frozen immediately on dry ice, and stored at –80°C until further processing. Then, single cell mRNA samples were reverse transcribed, and subsequently PCR amplified using target–specific probes. For internal controls, brain homogenates of the broader CeA region were also collected and purified using Trizol (Invitrogen). Tissue control samples were reverse transcribed and PCR amplified together with the single cell samples. Critical threshold cycles (Ct) values were then determined by using Taqman assays (Integrated DNA Technologies) and BioMark 48x48 Dynamic Array integrated microfluidic assays (Fluidigm Corporation). The resulting data were analyzed with custom scripts in Mathematica 9 (Wolfram Research), and plotted as normalized expression relative to housekeeping genes (*ActinB1*, *Atp1b1*, and *Hprt*, average of 3 genes) measured in the same cells. Cells where normalized mRNA values were < 10% were classified as non-expressing; cut-offs ranging from 5%–20% were tested and yielded similar results. The probes were designed to have similar amplicon lengths (100–120 bp) to minimize amplification bias during PCR. In some cases commercially designed probes (Integrated DNA Technologies) were also used as specified below. Probes for *Sst*, *Gad1*, *Gad2*, *Pdyn*, *ActinB1*, *Atp1b1*, and *Hprt* had previously been validated by our lab (Fuccillo et al., 2015); for other genes, multiple probes were tested. These yielded highly consistent results and the data were collapsed across probes to generate a single value for each gene. Following PCA, clusters were determined using the ''FindClusters'' function in Mathematica 9. For the analysis shown in Figure S5C, the percentage of SNL cells in each cluster was adjusted by a correction factor (39/89 = 0.438) to account for the fact that more cells were sampled for this condition (SNL n = 89, PAG n = 39, BNST n = 39).

Gene	Forward primer	Probe sequence	Reverse primer
Gad1	CTTGGCGTAGAGGTAATCAGC	CACGGTGCCCTTTGCTTTCCAC	GGACATCTTCAAGTTCTGGCT
Gad2	GCCTTGTCTCCTGTGTCATAG	TGCATCAGTCCCTCCTCTCTAACCA	CCTTGCAGTGTTCAGCTCT
Sst	GGCATCATTCTCTGTCTGGTT	AGTTCCTGTTTCCCGGTGGCA	AGACTCCGTCAGTTTCTGC
Pdyn	CATGTCTCCCACTCCTCTGA	TCAACCCCCTGATTTGCTCCCTG	GTGCAGTGAGGATTCAGGATG
Nts	GCTGAGAGAAGATGAGAGGAATG	CCAGGAGAGTCAGGCACACCAG	TCCAGGGCTCTCACATCTT
	CAATGCTGACCATCTTCCAG	CTCCCAGTGTTGAAAGGCCCTGC	CATTGACGTTATCAAGGATAT CTTCC
	AGATCTATTGACAAACATGCATACATC	CCTCCGTCTTGGAAAATGACCTTGCT	CCGGGCTGTTCACGTTATTTA
	Commercial Assay: Mm.PT.58.6655733		
Tac2	AGGATTGCTGAAAGTGCTGAG	TGATGTCTCCTTTGGTCCCACGC	TGTTCCTCTTGCCCATAAGTC
	AAAGGAGACATCACTTCCACAG	AACAGCCAACCAGACACTCCCA	TGTTCTCTTCAACCACGTCG
	Commercial Assay: Mm.PT.58.43752849		
Gal	CACTCTGGGACTTGGGATG	CGCTGTTCAGGGTCCAACCTCTC	GTCGCTAAATGATCTGTGGTTG
	Commercial Assay: Mm.PT.58.31536591		
PKCd	TGTGCTGTGAAGATGAAGGAG	TGTCTTCCCTCGCTCTGTGCTG	AACGTTGTCTTCCACTCAGG
	CACCACACTATCCCCGTTG	ATCATGGAGAAGCTATTCGAGAG GGACC	CCTGATGTTTCCTGTTACTCCC
	GCTGCCATCCACAAGAAATG	AAGATGGTGTCCCGGCTATTGGTG	CATGTCGATGTTGAAGCGTTC
	AAATGCCGGGAGAAGGTG	AACCAAGTGACCCAGAGATCTTCCC	ACTCTGTTGTGTCCAGCTTC
	Commercial Assay: Mm.PT.58.10644503		
ActinB1	ATGCCGGAGCCGTTGTC	CCGCCACCAGTTCGCCATG	GCGAGCACAGCTTCTTTG
Atp1b1	GGCAGGACATTTGGATTATACTTC	TCATTCTTGGGAGGCTTCGGTTTGA	TCATTATCAAGCTCAACCGAGT
Hprt	AACAAAGTCTGGCCTGTATCC	CTTGCTGGTGAAAAGGACCTCTCGAA	CCCCAAAATGGTTAAGGTTGC

QUANTIFICATION AND STATISTICAL ANALYSIS

Statistical methods

Full statistical information is provided in Table S1. Data were plotted with Excel (Microsoft), Prism (GraphPad) or MATLAB and analyzed statistically with SigmaStat (Systat), MATLAB, or Mathematica (Wolfram). Parametric tests (t tests; ANOVAs followed by Student-Newman-Keuls or Holm-Sidak post hoc tests) were used in cases where data met assumptions of normality and equal variance. In cases where data did not conform to these assumptions, non-parametric tests (Wilcoxon signed-rank or Mann-Whitney rank sum tests; Friedman's repeated-measures ANOVA on ranks followed by Student-Newman-Keuls post hoc tests) were used.

Analysis and quantification of behavioral data

CS-evoked freezing during fear conditioning was scored manually. For loss-of-function fear conditioning studies where comparisons were made between groups, the experimenter scoring behavior was blinded to group identity. For all other studies, behavioral data was collected automatically by a computer using commercial software (MedPC or Biobserve). Although experimenters were not blinded to group assignment, identical procedures were followed for data collection and groups were counterbalanced and interleaved.

Analysis and quantification of photometry data

Raw data from 490nm and 405nm channels were passed through a zero-phase digital filter (*filtfilt* function in MATLAB) and a least-squares linear fit (parameters derived with *polyfit* function) was applied to the 405nm control signal to align it to the 490nm signal. ΔF/F was calculated with the following formula: (490nm signal - fitted 405nm signal) / (fitted 405nm signal). To facilitate comparisons across animals, Z-scores were calculated by subtracting the mean ΔF/F calculated across the entire session and dividing by the standard deviation $[(\Delta F/F - \overline{\Delta F/F})/(\sigma \Delta F/F)]$. Peri-stimulus time histograms (PSTHs) were created using the TTL timestamps corresponding to behavioral events. Rewarded port entries were defined as the first entry following reward, unless the mouse was already in the port at the time of reward delivery in which case the moment of sucrose pump activation was used. Unrewarded port entries were defined as entries occurring > 20 s before or after rewarded entry times to prevent unwanted overlap of neural data for these events. To avoid re-sampling the same data with slight time shifts when multiple unrewarded entries occurred in bursts, only 1 unrewarded entry within a 20 s window was included in the PSTH (the first event was chosen). For lever presses, the same approach was used to avoid re-sampling data during bursts of lever pressing: neural data from 1 press per 1 s time window was

included in the PSTH. The mean Z-score during pre- and/or post-event time windows (length specified in figure legends, generally 5 or 10 s) was quantified for statistical comparison across animals. The window length was chosen to capture the majority of post-event neural activity evident in the group average data, and an equivalent pre-event window was taken. For quantitative CS-US comparisons, due to the different temporal kinetics of these responses, instead of calculating the mean Z-score during a fixed time window, the time corresponding to the peak response was determined and the mean signal in a 1 s window following the peak was quantified.

DATA AND CODE AVAILABILITY

The code generated during this study is available at https://github.com/elizabeth-steinberg. Raw data are available from the corresponding author on request.